CANCER

M2 macrophages drive leukemic transformation by imposing resistance to phagocytosis and improving mitochondrial metabolism

Isabel Weinhäuser[1,2,3], Diego A. Pereira-Martins[1,2,3], Luciana Y. Almeida[2], Jacobien R. Hilberink[1], Douglas R. A. Silveira[4], Lynn Quek[4], Cesar Ortiz[2,3], Cleide L. Araujo[2], Thiago M. Bianco[2], Antonio Lucena-Araujo[5], Jose Mauricio Mota[6], Shanna M. Hogeling[1], Dominique Sternadt[1], Nienke Visser[1], Arjan Diepstra[7], Emanuele Ammatuna[1], Gerwin Huls[1], Eduardo M. Rego[3]*, Jan Jacob Schuringa[1]*

It is increasingly becoming clear that cancers are a symbiosis of diverse cell types and tumor clones. Combined single-cell RNA sequencing, flow cytometry, and immunohistochemistry studies of the innate immune compartment in the bone marrow of patients with acute myeloid leukemia (AML) reveal a shift toward a tumor-supportive M2-polarized macrophage landscape with an altered transcriptional program, with enhanced fatty acid oxidation and NAD^+ generation. Functionally, these AML-associated macrophages display decreased phagocytic activity and intra–bone marrow coinjection of M2 macrophages together with leukemic blasts strongly enhances in vivo transformation potential. A 2-day in vitro exposure to M2 macrophages results in the accumulation of $CALR^{low}$ leukemic blast cells, which are now protected against phagocytosis. Moreover, M2-exposed "trained" leukemic blasts display increased mitochondrial metabolism, in part mediated via mitochondrial transfer. Our study provides insight into the mechanisms by which the immune landscape contributes to aggressive leukemia development and provides alternatives for targeting strategies aimed at the tumor microenvironment.

INTRODUCTION

Acute myeloid leukemia (AML) is a complex and aggressive disease characterized by a high genetic heterogeneity and clonal diversity across and even within patients (*1*–*4*). The expansion of AML leukemic stem cells (LSCs) and their progeny rapidly usurps the bone marrow (BM) niche to impede healthy hematopoiesis, reshape BM-derived stromal cell function, and escape immune surveillance (*5*–*7*). Much like healthy hematopoietic stem cells (HSCs), LSCs reside in BM niches to ensure their survival, facilitate AML progression, and escape cytotoxic therapy (*8*–*10*).

Within the BM niche, macrophages can regulate the fate of HSCs during homeostasis. In vivo macrophage depletion promotes increased mobilization of HSC (*11*). Hur *et al.* (*12*) revealed that $CD234^+$ macrophages can interact with $CD82^+$ long-term (LT) HSCs to support quiescence in the endosteal region, while others identified erythroblastic island macrophages to promote erythropoiesis (*13*, *14*). Thus, the BM harbors diverse macrophage populations, which can be exploited by HSCs or LSCs. In this context, Mussai *et al.* (*15*) detected increased Arginase 2 activity released from AML blast cells to promote M2 macrophage polarization and inhibit T-cell proliferation. Using AML murine models, Al-Matary *et al.* (*16*) observed increased infiltration of monocytes/macrophages with pro-leukemogenic functions and identified the transcriptional repressor *Gfi1* to regulate M2 polarization. Last, a recent single-cell RNA sequencing (scRNA-req) study revealed that the heterogeneity of AML is not only inherent to the leukemic blast population but also extends to the stromal and immune cells within the BM (*17*). By analyzing 16 patients with AML, the authors identified 10 macrophage subpopulations with immunosuppressive features.

Here, we show that AML-derived macrophages present immunosuppressive and pro-leukemogenic functions, in part related to the acquisition of AML mutations. We observe strong heterogeneity in the macrophage landscape across patients with AML, and patients harboring a large M2-polarized macrophage compartment display dismal prognosis, which is associated with low expression of *CALR* and a more stem-like phenotype of leukemic blasts, coupled with intrinsic resistance to phagocytosis. Functionally, we show that M2-polarized macrophages drive aggressive in vivo leukemia development of primary AML and of acute promyelocytic leukemia (APL) cells, which are otherwise notoriously difficult to engraft in xenograft models. Furthermore, direct interaction with M2-polarized macrophages enhances homing and alters metabolism via the direct exchange of mitochondria from macrophages to leukemic blasts. We provide insight into the mechanisms by which M2-polarized macrophages contribute to aggressive leukemia development and provide alternatives for targeting strategies.

[1]Department of Experimental Hematology, Cancer Research Centre Groningen, University Medical Centre Groningen, University of Groningen, Groningen, Netherlands. [2]Department of Internal Medicine, Medical School of Ribeirao Preto, University of São Paulo, Ribeirao Preto, Brazil. [3]Center for Cell Based Therapy, University of São Paulo, Ribeirao Preto, Brazil. [4]Myeloid Leukaemia Genomics and Biology Group, School of Cancer and Pharmaceutical Sciences, King's College London, London, SE5 8AF, UK. [5]Department of Genetics, Federal University of Pernambuco, Recife, Brazil. [6]Medical Oncology Service, Sao Paulo State Cancer Institute, University of Sao Paulo, Brazil. [7]Department of Pathology and Medical Biology, Cancer Research Centre Groningen, University Medical Centre Groningen, University of Groningen, Groningen, Netherlands.
*Corresponding author. Email: eduardo.rego@fm.usp.br (E.M.R.); j.j.schuringa@umcg.nl (J.J.S.)

RESULTS

The macrophage landscape is heterogeneous in AML

To evaluate the transcriptional differences between AML-associated macrophages (AAMs) and macrophages isolated from healthy donors (HDs), we performed an unsupervised cluster analysis using scRNAseq data (GSE116256). Our analysis identified 19 clusters, of which 5 were composed of cells enriched for macrophage signatures (fig. S1, A and B). Seurat analysis of these cells (7030 AAMs and 814 healthy BM macrophages) resulted in the identification of 12 subclusters (Fig. 1, A and B), two of which were detected in both healthy individuals and patients with AML (K0 and K4), three clusters were overrepresented in healthy individuals (K5, K6, and K10), and seven were AML specific (Fig. 1C). When we evaluated the patient-specific contributions to all 12 clusters, we observed that different patients contributed to most clusters, except for AML921A.D0 from which clusters 1 to 3 and 8 arose and AML419A.D0 from which clusters 11 and 7 arose (fig. S1C). Differential gene expression analysis within subclusters revealed up-regulation of 306 genes in AAMs associated with biological pathways such as proliferation, inflammation, and cellular metabolism (Fig. 1D and tables S1 to S5). Among the up-regulated genes, we identified the M2 markers such as *CD163* and *MRC1* (which encodes the CD206), the major fatty acid (FA) transporter *CD36*, the nicotinamide phosphoribosyltransferase (NAMPT), and the exocyst protein EXOC5 (Fig. 1, D and E).

We then analyzed CD163, CD206, and CD36 expression in a large cohort of primary AML patient samples using multiparametric flow cytometry analysis (Table 1). These markers were strongly expressed in AML, particularly in the more mature $SSC^{high}CD45^{high}$HLA-$DR^{+}CD14^{+/-}CD16^{+/-}$ AML myeloid subpopulation compared to the immature blast compartment (Fig. 1, F and G). Compared to HDs, we observed that the percentage of M2-like $CD163^{+}CD206^{+}$ macrophages was significantly increased, while the level of M1-like $CD80^{+}$ macrophages was significantly decreased compared to HD, albeit that strong heterogeneity among patients with AML was also observed (Fig. 1H). Notably, we did observe that the separation of blasts in which LSCs reside from AAMs can be more challenging in more committed M4/M5 or monocytic AML subtypes. To ensure that the quantification of macrophages in the BM by flow cytometry would not result in an underrepresentation due to difficulties in efficiently retrieving macrophages using BM aspirates, we performed an immunohistochemistry staining for CD163, which indicated no significant differences between the two techniques (Fig. 1I). CD163 and CD206 expression was associated with worse clinical outcome, similar to previous studies based on mRNA levels (*2*, *18*, *19*), and here we also demonstrate that these prognostic M2-markers act independently of main clinical prognosticators such as age, sex, and leukocyte counts (fig. S1D and Table 2).

Considering that our single-cell analysis depicts a heterogeneity of AAM that goes beyond the up-regulation of CD163 and CD206 and considering that the CIBERSORT-defined macrophage signatures are based on solid tumors, we decided to generate an M2-AAM signature specifically for AML. First, we selected genes exclusively expressed by M2 macrophages (92 genes) from four different datasets (FANTON, BLUEPRINT, CIBERSORT, and HPCA) (fig. S1E). From these 92, five genes (*MRC1*, *CD163*, *FGR*, *GASK1B*, and *RASA3*) could predict overall survival (OS) in at least two AML cohorts and were differentially expressed between the paired $CD34^{+}$ or $CD34^{-}$ compartments of patients with AML [except for *MRC1*, mainly due to monocytic blasts (*20*)] (fig. S1F). We next used the combined gene expression of these five AAM-associated genes to design a prognostic score (M2-AAM signature) to stratify patients with AML regarding clinical outcomes. The M2-AAM signature could independently predict poorer clinical outcomes in The Cancer Genome Atlas (TCGA) AML cohort considering European LeukemiaNet (ELN)–risk stratification, age, and sex as confounders (fig. S1G). In addition, our M2-AAM signature was also able to predict progression-free survival (PFS) in a cohort of patients with myelodysplastic syndrome (MDS) (fig. S1H). These results were specific to the M2 signature and independent of the revised International Prognostic Scoring System (fig. S1I). Thus, our data suggest that AAM can exacerbate the progression of a pre-leukemic and leukemic state and indicate that the quantification and classification of AAM at diagnosis can improve AML and MDS risk stratification and clinical decision-making.

AAMs display impaired phagocytic activity

To further explore functional differences between AAMs and healthy macrophages, we performed a single-cell gene set enrichment analysis (scGSEA), which revealed enrichment for an M2-polarized macrophage signature, FA metabolism, and immunosuppression in AAMs (Fig. 2, A and B, and table S6). Next, we isolated AAM from biobanked AML samples and evaluated their immune function in comparison to HD-derived macrophages. Phagocytosis assays were performed with AAM isolated from frozen AML samples (by adherence) and carboxyfluorescein succinimidyl ester (CSFE)–labeled leukemic MV4-11 cells. Phagocytosis activity of AAMs differed considerably across different patient samples. AAMs were then dichotomized into high and low phagocyting AAM based on the median value (0.52) of the fold change (FC) of AAM compared to the control, whereby AAMs 6 to 13 displayed low phagocytic capacity (Fig. 2C). When we analyzed the macrophage profile of these patients at baseline, we noticed that phagocytic capacity of AAMs positively correlated with the percentage of CD80 detected on AAMs and also with the total of $CD80^{+}$ AAMs found in the BM (fig. S2A). These results further highlight the heterogeneity in the AML macrophage landscape.

Considering that AAM can directly derive from the mutated leukemic clone, we sorted and sequenced the $CD45^{dim}$HLA-$DR^{-}CD14^{-}CD163^{low}$ (leukemic blasts) and $CD45^{high}$HLA-$DR^{+}CD14^{+}CD163^{high}$ (AAM) of AML samples. Sequencing analysis indicated that AML mutations present in the leukemic blast were also detected in the AAM populations (n = 5 independent AML samples; fig. S2, B to D). Morphological analysis of $CD45^{dim}$HLA-$DR^{-}CD14^{-}CD163^{low}$ cells indicated an increased nucleus: cytoplasm ratio, a more open chromatin structure, and visible nucleoli, characteristic of myeloblastic cells. The $CD45^{high}$HLA-$DR^{+}CD14^{+}CD163^{high}$ population presented with a lower nucleus: cytoplasm ratio and a more condensed chromatin structure with a lobular aspect, which is distinctive for more differentiated cells (fig. S2B). To determine how recurrent AML mutations might affect the phagocytosis capacity of AAMs, we lentivirally transduced cord blood (CB)–derived $CD34^{+}$ with various genetic alterations commonly found in patients with AML, such as *fms-like tyrosine kinase 3 internal tandem duplication* (*FLT3-ITD*), cytoplasmic *nucleophosmin 1* (*NPM1*cyt), *BCR-ABL*

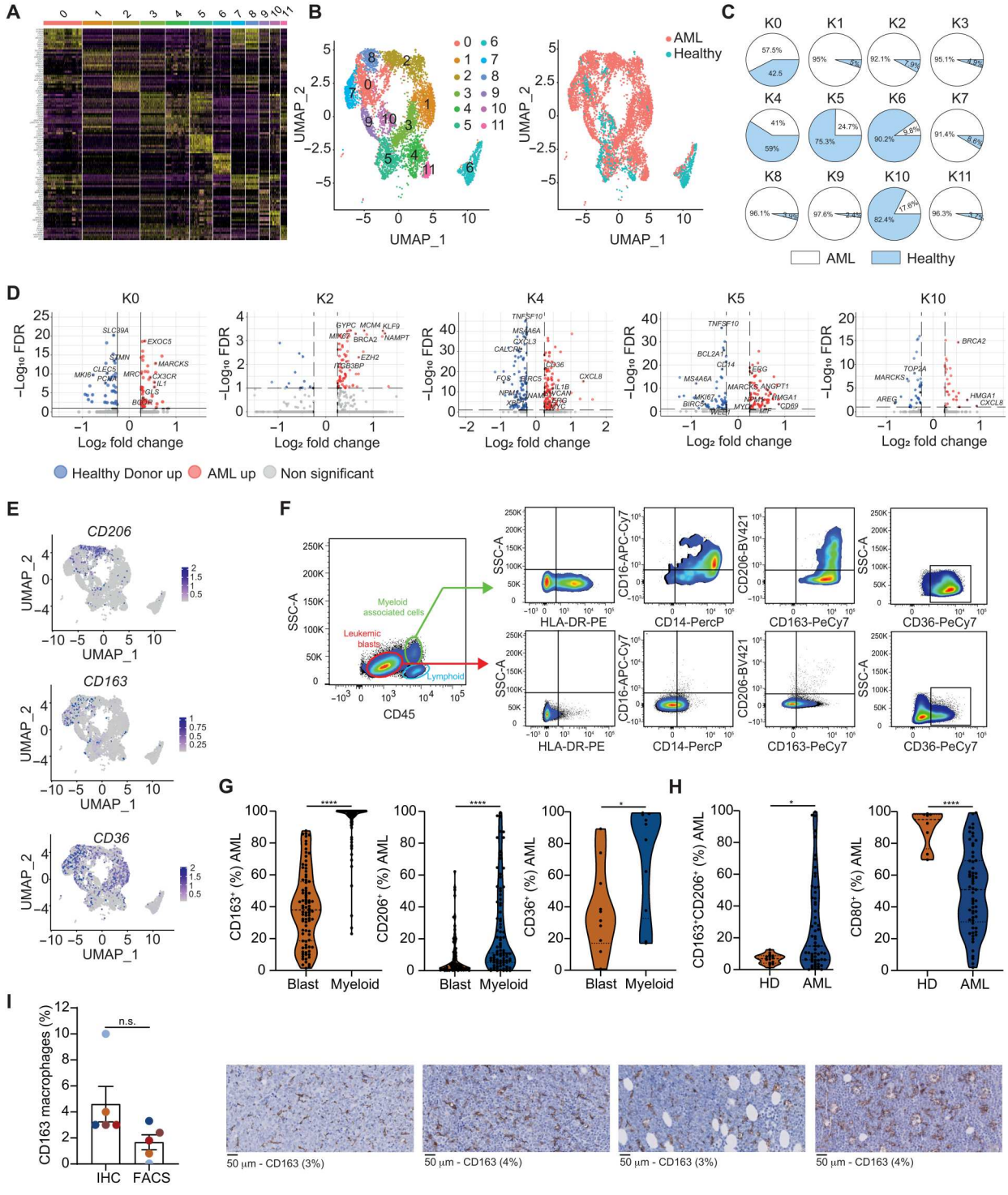

Fig. 1. Heterogeneity within the macrophage landscape in AML. (**A**) Heatmap displaying the differentially expressed genes used to perform the SEURAT analysis (scRNA-seq GSE116256). (**B**) UMAP projection of monocytic/macrophage-like BM cells from nine patients with AML and two HDs, showing the formation of 12 main clusters. (**C**) Pie charts representing the frequency distribution of cells in each cluster, regarding the sample origin (HD versus AML). (**D**) Volcano plot demonstrating the differentially expressed genes in monocytes/macrophages from patients with AML compared to healthy BM donors. (**E**) UMAP projection of differentially expressed genes in AAMs associated with an M2-like phenotype. (**F**) Representative FACS plots of macrophage marker expression in different AML CD45$^+$ subpopulations. (**G**) The expression of macrophage markers in the AML blasts (SSC^{low}CD45^{dim}) versus the mature myeloid population (SSC^{high}CD45^{high}). (**H**) The amount of CD163$^+$CD206$^+$ macrophages detected in patients with AML compared to HDs. (**I**) The amount of CD163$^+$ macrophages quantified by immunohistochemistry (IHC) and FACS. Representative IHC pictures for CD163 in AML biopsies. (G and I) Wilcoxon signed rank test (two-sided); n.s., nonsignificant; *P < 0.05 and ****P < 0.0001. (H) Mann-Whitney test for unpaired data (two-sided). *P < 0.05 and ***P < 0.001. (G to I) Each dot represents an individual patient.

Table 1. Clinical characteristics of patients with AML included. FAB, French-American-British classification; ELN, European Leukemia-Net; FLT3, Fms-related receptor tyrosine kinase 3 gene; ITD, internal tandem duplication; TKD, tyrosine kinase domain; HSCT, hematopoietic stem cell transplant; CHR, complete hematological remission; CRi, incomplete remission.

Characteristics	All patients, 88 patients		
	No.	%	Median (range)
Gender			
Female	43	54.4	
Male	36	45.6	
Unknown	9	–	
Age, years			60.7 (21, 86)
18–40	10	14.5	
41–60	22	31.9	
≥60	37	53.6	
Unknown	19	–	
Leukocyte counts, $\times 10^9$/liter			61.4 (1.5, 335.6)
Platelet counts, $\times 10^9$/liter			41.5 (2, 281)
Hemoglobin, g/dl			5.8 (3.2, 11.4)
BM blasts, %			76 (3, 99)
Lactate dehydrogenase, U/dl			655.5 (197, 4632)
FAB classification			
M1	18	32.1	
M2	5	8.9	
M3	17	30.4	
M4	7	12.5	
M5	9	16.1	
Unknown	32	–	
ELN2017 risk stratification			
Favorable	15	24.2	
Intermediate	32	51.6	
Adverse	15	24.2	
Unknown	26	–	
FLT3 mutational status			
Non-mutant	35	57.4	
ITD/TKD mutant	25	42.6	
Missing	28	–	
HSCT status			
Yes	39	66.1	
No	20	33.9	
Unknown	29	–	
Treatment scheme			
Intensive chemotherapy (3 + 7)	48	76.2	
Hypomethylating agents	12	19	
Best supportive care	3	4.8	
Unknown	25	–	
Treatment response			
CHR	42	72.4	
CRi	7	12.1	
No response/refractory	9	15.5	

continued on next page

Characteristics	All patients, 88 patients		
	No.	%	Median (range)
Unknown	30	–	
Relapse status			
Relapse	15	25	
Nonrelapse	45	75	
Unknown	28	–	
Survival status			
Dead	48	70.6	
Alive	20	29.4	
Unknown	20	–	
Macrophage clusters			
High M2 macrophage	14	45.2	
Low M2 macrophage	17	54.8	
Unknown	57	–	

p210, meningioma (*MN1*) overexpression, and knockdown (KD) of *DNA* (*cytosine-5*)–*methyltransferase 3A* (*DNMT3A*) (mimicking the loss of function observed in patients with *DNMT3A* mutations) and differentiated them toward M0 macrophages. Among all the groups, CB-derived *FLT3*-ITD$^+$ and *DNMT3A*-KD macrophages displayed a decreased phagocytic activity compared to HD controls (Fig. 2D), indicating that AML mutations acquired by macrophages can affect their immune function. When we evaluated the expression of macrophage cell surface markers, we observed no differences between the different mutations except for CB-derived *FLT3*-ITD$^+$ macrophages, which displayed increased expression of CD206 and CD80 (fig. S2F). Furthermore, no differences in cell morphology or cell cycle state were observed upon the introduction of the genetic alterations when compared to empty vector control (Fig. 2E and fig. S2G). In conclusion, these data indicate that AAMs can display an immunosuppressive phenotype with impaired immune functions, which can be caused in part by the acquisition of AML mutations in the macrophage compartment.

Intrabone coinjection of M2 macrophages strongly supports in vivo leukemia progression

Next, we decided to evaluate how macrophages can support leukemic growth. Since extensive functional studies with primary AAMs are challenging due to the limited cell numbers that can be obtained, we continued to study the impact of macrophages on primary AML blasts using healthy peripheral blood (PB)–derived interleukin-6 (IL-6)–polarized M2d macrophages. In earlier studies, we also performed extensive in vitro experiments with IL-4–polarized M2a macrophages, which gave essentially similar results as M2d macrophages, but since phenotypes were more dominant with M2d macrophages, we continued our experiments with those. Fluorescence-activated cell sorting (FACS) analysis confirmed high expression of CD163 and CD206 in M2d-polarized macrophages, while CD80 expression was high in M1-polarized macrophages (fig. S2H). In vitro, LT co-cultures promoted increased proliferation of primary AML cells when cultured on M2 macrophages compared to cultures on MS5 BM stromal cells [strong AML expanders (Fig. 2F) and weaker AML expanders (fig.S2I)], which was not observed with

Table 2. Univariable and multivariable analyses. Hazard ratios (HRs) > 1 or < 1 indicate an increased or decreased risk, respectively, of an event for the first category listed. DFS, disease-free survival; ELN, European Leukemia-Net; HR, hazard ratio.

Endpoint	Model variables	Univariable analysis				Multivariable analysis			
		HR	95% CI		*P* value	HR	95% CI		*P* value
OS (*n* = 28)	Macrophage clusters: high M2 versus low M2	2.52	1.003	6.36	0.04	2.74	1.01	7.4	0.04
	ELN2017-risk stratification: favorable versus intermediate versus adverse	1.48	0.69	3.13	0.305	2.16	0.97	4.75	0.057
	Age at diagnosis: continuous variable	1.03	0.99	1.07	0.098	1.01	1.004	1.12	0.035
DFS (*n* = 20)	Macrophage clusters: high M2 versus low M2	3.47	1.15	10.47	0.027	3.23	1.03	10.07	0.043
	ELN2017-risk stratification: favorable versus intermediate versus adverse	0.83	0.35	1.96	0.677	1.33	0.52	3.41	0.543
	Age at diagnosis: continuous variable	1.03	0.99	1.08	0.121	1.05	0.98	1.12	0.117

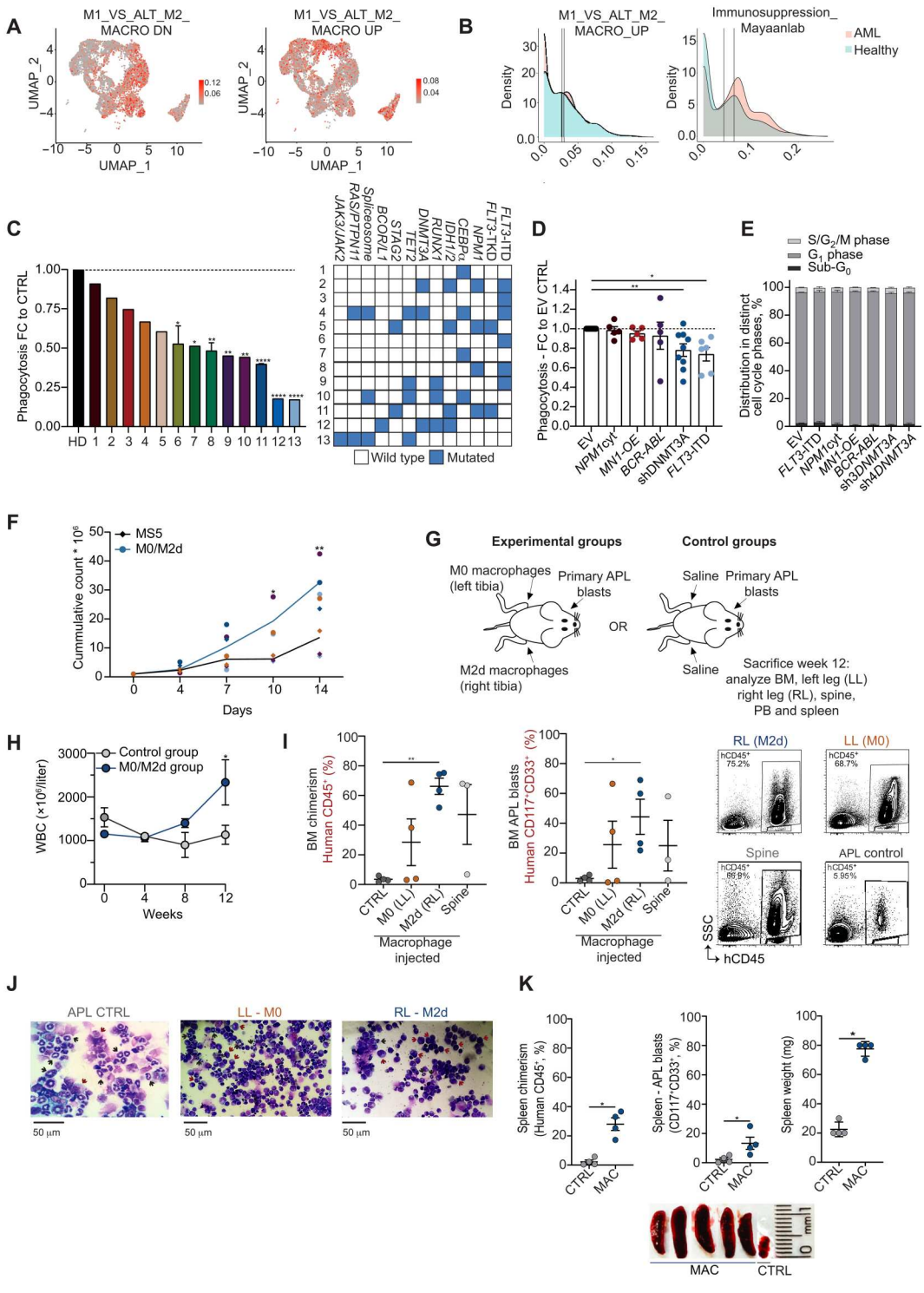

Fig. 2. AAMs display impaired phagocytic activity. (**A**) Single-cell scGSEA projection in the macrophage landscape of patients with AML and HD. (**B**) Density plots displaying the enrichment scores for the scGSEA. (**C**) Bar plot displaying the fold change of phagocytosed carboxyfluorescein succinimidyl ester (CSFE)–labeled MV4-11 cells by HD (CTRL) and AAM. Oncoprint displaying the baseline mutations of the patients with AML from which macrophages were isolated. (**D**) Bar plot displaying the fold change compared to control of phagocytosed CSFE-labeled MV4-11 cells by empty vector control and *NPM1*cyt, *MN1*-overexpression, *BCR-ABL*, sh*DNMT3A*, *FLT3*-ITD (W81) CB-derived transduced macrophages. (**E**) Cell cycle analyses of macrophages derived under (D). (**F**) Cumulative cell count of primary AML cells cultured on M0/M2d macrophages (closed circles) or MS5 (control, diamonds) for 14 days. Similar colors indicate similar patient samples. (**G**) In vivo coinjection experimental setup. (**H**) Leukocyte count in transplanted mice ($n = 4$). WBC, white blood cell. (**I**) Bar graphs of the percentage of human CD45$^+$ (left) and human APL blast cells (CD117$^+$CD33$^+$) (right) detected in the BM of mice without (control) or with coinjected macrophages ($n = 4$). LL, left leg; RL, right leg, injected with M0 and M2d macrophages, respectively. Representative FACS plot. The material of one mouse was excluded from the BM/spleen chimerism data due to low cell viability. (**J**) BM representative cytospins of control and coinjected mice. Arrows indicate human APL blast cells. (**K**) Human CD45$^+$ and APL blasts (CD117$^+$CD33$^+$) cells (%) detected in the spleen ($n = 4$) and spleen weight. Representative spleen pictures of mice injected without (control) and with macrophages (Mac). (C, D, and E) Kruskal-Wallis test. (I) Independent sample *t* test. (F and H) Two-way analysis of variance (ANOVA). (K) Mann-Whitney test for unpaired data (two-sided). (D, F, I, and K) Each dot represents an individual patient. Data indicate the SEM. *$P < 0.05$, **$P < 0.01$, and ****$P < 0.0001$.

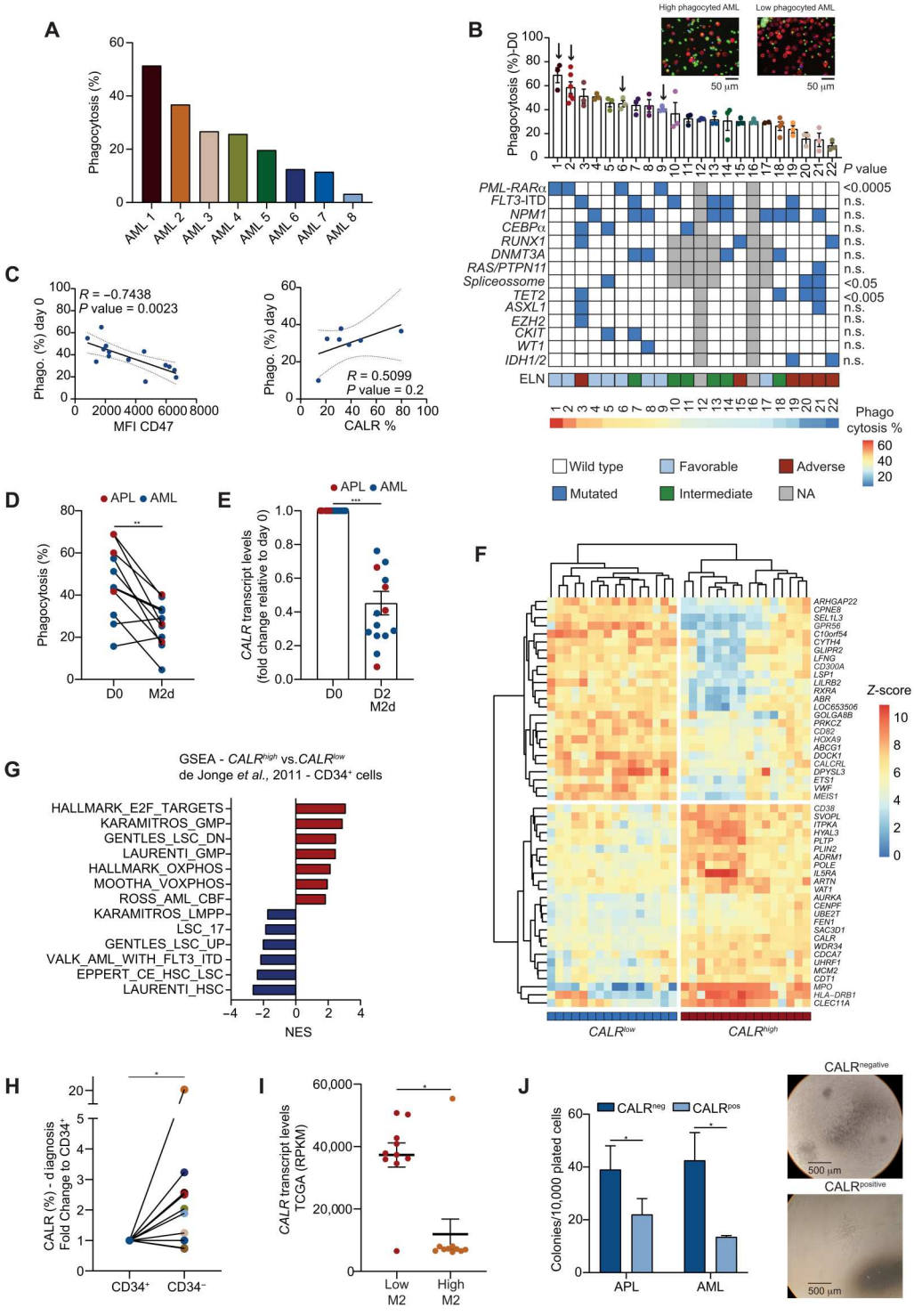

Fig. 3. Heterogeneity in intrinsic phagocytosis sensitivity across leukemia samples is associated with CALR expression and maturation stage. (**A**) Bar plot displaying the percentage of phagocytosed CSFE-labeled primary AML cells by murine (NSG-isolated) macrophages. (**B**) Bar plot displaying the percentage of phagocytosed CSFE or Incucyte Red–labeled primary AML cells by human PB-derived macrophages. Oncoprint displaying the baseline mutations and ELN2022-risk stratification of the patients with AML. NA, not available. (**C**) Pearson correlation between the level of phagocytosis measured at diagnosis and the CD47 mean fluorescence intensity (MFI) level, as well as the percentage of CARL, measured on the respective AML blast population ($SSC^{low}CD45^{dim}CD34^{+}$ or $CD117^{+}$ for $CD34^{-}$ AMLs). (**D**) Phagocytosis of primary AML at diagnosis and after 48 hours of co-culture on M2d macrophages. (**E**) *CALR* transcript level of primary AML at diagnosis (D0) and after a 48-hour coculture on M2d macrophages. Data are represented as a fold change to diagnosis (D0) levels. D0, day 0/diagnosis. (**F**) Heatmap of genes differentially expressed between $CALR^{low}$ and $CALR^{high}$ patients analyzed on the transcriptome of $CD34^{+}$-sorted AML cells (GSE30029). (**G**) GSEA of $CALR^{low}$ and $CALR^{high}$ patients analyzed on the transcriptome of $CD34^{+}$-sorted AML cells. NES, normalized enrichment score. (**H**) FACS measured expression of CALR in $CD34^{+}$ and $CD34^{-}$ leukemic blast cells. (**I**) M2-AAM score in patients with the highest (10 patients) and lowest (10 patients) expression of CALR in the TCGA set. (**J**) Colony formation of $CALR^{neg}$ and $CALR^{pos}$ cells sorted from primary APL/AML blast cells within the SSC^{low} $CD45^{dim}$ fraction. Representative colonies of $CALR^{neg}$ and $CALR^{pos}$ cells. $CALR^{neg}$, calreticulin negative; $CALR^{pos}$, calreticulin positive. (B to E and H to I) Each dot represents an individual patient. (B) Mann-Whitney test for unpaired data (two-sided). (D, E, H, and J) Wilcoxon signed rank test (two-sided). $^{*}P < 0.05$, $^{**}P < 0.01$, and $^{***}P < 0.001$. Data indicate the SEM.

healthy hematopoietic stem/progenitor cells (HSPCs) (fig. S2J). The addition of M2d-conditioned medium to AML-MS5 cocultures was not sufficient to enhance proliferation, suggesting that direct cell-to-cell contact with macrophages is relevant (fig. S2K).

Considering that patient-derived xenograft (PDX) models, especially for favorable/intermediate subtypes, remain a challenge in AML, we questioned whether the presence of a tolerogenic microenvironment could allow or boost the engraftment of those AMLs. To eliminate the heterogeneity of AML samples, we decided to start with the favorable, highly homogeneous (*21*) and particularly difficult to engraft subtype (*22*) APL. In a first set of experiments, we injected human PB-derived nonpolarized (M0) and M2d-polarized macrophages into the BM of NOD.Cg-Prkdc^{scid} Il2rg^{tm1Wjl} Tg(CMV-IL3,CSF2,KITLG)1Eav/MloySzJ (NSGS) mice

followed by the transplant of primary APL cells via the retro-orbital route. Control mice only received primary APL cells (Fig. 2G). As expected, none of the mice receiving APL blasts without macrophages succumbed to leukemia (Fig. 2, H to K). In stark contrast, at week 12 after transplant, mice injected with M0 and M2d macrophages presented leukocytosis indicating the manifestation of leukemia (Fig. 2H). Mice were euthanized at week 12 to determine the level of human APL blasts in each leg and spine (as an internal control). The percentage of human $CD45^+$ cells and $CD117^+CD33^+$ APL blasts was increased in macrophage-injected mice compared to controls, most notably in M2d-injected legs (Fig. 2I). Engrafted BM cells displayed human promyelocyte characteristics (Fig. 2J). In line with leukemia onset, APL blast infiltrated the spleen of macrophage recipient mice resulting in increased spleen weight (Fig. 2K). These data indicate that alterations in the BM niche can affect the progression of leukemia and suggest that the presence of an immune-supportive environment can facilitate the engraftment of favorable AML samples.

Heterogeneity in intrinsic phagocytosis sensitivity across leukemia samples is associated with CALR expression and maturation stage

We wondered whether the exogenous healthy macrophages present in immunodeficient mouse strains, which are typically displaying a tumor-suppressive phenotype, would act as an immune barrier compromising human AML engraftment. First, we tested whether macrophages isolated from NSG mice were able to phagocytose primary AML blasts. These macrophages could phagocytose AML blasts with efficiencies ranging between 3.2 and 51.4% (Fig. 3A), similar to phagocytosis levels observed when using human M0 macrophages for the same AML samples (fig. S3A). Since we did observe a clear heterogeneity in intrinsic phagocytosis sensitivity between AML samples, we then extended the panel of AMLs in our phagocytosis assays using human M0 macrophages and also included primary APL samples. Despite the limited amount of samples, we observed a tendency of APL samples (samples 1, 2, 6, and 9) to be more intrinsically sensitive to phagocytosis, while AML samples with spliceosome-related (*SF3B1*, *U2AF1*, and *SRSF2*), *tet methylcytosine dioxygenase* 2 (*TET2*), or *isocitrate dehydrogenase 1/2* (*IDH1/2*) mutations appeared to be less sensitive (Fig. 3B). Notably, these data should be interpreted with caution, and validation studies are needed to corroborate the suggestive phenotype-to-genotype associations. "Don't eat me signals" CD47 (*23*) or CD24 (*24*) were negatively correlated with AML phagocytosis (Fig. 3C and fig. S3B), while there was a positive correlation between cell surface expression of the "eat me signal" calreticulin (CALR) and AML phagocytosis (Fig. 3C). When comparing the transcript levels of *CALR* and *CD47* using TCGA bulk RNA-seq data of different leukemia subtypes, APL samples presented with the highest level of *CALR* expression, potentially in line with their high intrinsic phagocytosis sensitivity, while no substantial differences were observed for *CD47* (fig. S3C). Also at the scRNA level, no correlation between the expression of *CALR* and *CD47* was observed (fig. S3, D and E), in line with our flow cytometry experiments (fig. S3F).

Furthermore, we noticed a negative correlation between the size of the myeloid compartment detected in the AML samples (as determined by the % of AAM) and their susceptibility to phagocytosis (fig. S3G). These data suggested that leukemic cells, once exposed to macrophages in the BM, would be more apt to evade the innate immune system. To functionally test this hypothesis, we co-cultured AML blasts on M2d macrophages for 2 days after which the remaining cells were harvested and used for a new phagocytosis assay on fresh macrophages. Compared to the level of phagocytosis of uncultured cells (on average 40%), we observed a significant reduction in phagocytosis when leukemic blasts were "trained" on M2d macrophages (Fig. 3D), as well as a significant reduction in *CALR* transcript levels (Fig. 3E). No difference in the expression of the "don't eat me signal" CD47 was observed (fig. S3H). In addition, we performed a differential gene expression analysis of $CALR^{high}$ versus $CALR^{low}$ patients using the transcriptome of $CD34^+$-sorted AML blast cells (AAM depleted) (*25*). Principal components analyses revealed a clear separation between $CALR^{high}$ and $CALR^{low}$ samples (fig. S3I). Furthermore, $CALR^{low}$ patients displayed increased expression of genes associated with stem-like features such as *GPR56* (*26*), *CD300A* (*27*), *CD82* (*12*), *HOXA9* (*28*), *CALCRL* (*29*), and *MEIS1* (*30*) (Fig. 3F, highlighted in bold). Reversely, genes associated with myeloid cell differentiation such as *MPO* and *CD38* were up-regulated in the $CALR^{high}$ group (Fig. 3F, highlighted in bold). GSEA associated $CALR^{low}$ AMLs with the terms "L-HSC/LMPP" and "17-LSC," while $CALR^{high}$ samples were associated with the terms "L-GMP/CMP," "core binding factor (CBF) leukemias", and "oxidative phosphorylation (OXPHOS)" (Fig. 3G). Flow cytometry analysis also indicated that $CD34^+$ cells exhibited significantly lower expression of CALR compared to more committed $CD34^-$ cells (Fig. 3H). Furthermore, we observed lower *CALR* transcript levels in patients displaying a high M2-AAM signature (Fig. 3I). Last, we sorted the $CALR^-$ and $CALR^+$ populations (fig. S3J) of two patients with AML, one of which was diagnosed with APL, and evaluated their colony formation capacity. In accordance with our transcriptome analysis, our results showed increased colony formation by $CALR^-$ compared to $CALR^+$ (Fig. 3J). In summary, our data suggest that the exposure of AML cells to M2 macrophages in the BM as well as in vitro promotes the selection of a more stem-like leukemic cell with immune evasive characteristics, which is associated with a downregulation of CALR.

Coculture of non-engrafting APL cells on M2 macrophages induces full-blown leukemia in a xenograft model

Our in vitro data indicated that leukemic blasts can undergo two fates when encountering M2-polarized macrophages: They are either phagocytosed or not, in which case cells have altered characteristics including improved immune evasion. Next, we questioned whether short-term exposure of primary APL cells to M2 macrophagesin vitro would be sufficient to improve their ability to engraft. Primary human and murine APL cells were cocultured on human PB-derived or murine BM-derived M0 or M2d macrophages for 48 hours. Subsequently, a substantial fraction of leukemic blasts were phagocytosed leaving 8.3 and 10.5% of the original input of human and murine blasts, respectively (fig. S4, A and B). Next, we injected 1.5×10^5 trained cells retro-orbitally into NSGS mice. As controls, cells were pre-cultured on mesenchymal stromal cells (MSCs) or mice received 1×10^6 non-cultured cells (Fig. 4A). Notably, only human APL cells pre-cultured on macrophages were able to induce full-blown leukemia (Fig. 4, B to F). Freshly transplanted APL cells or pre-cultured blasts on MSCs did not induce leukemia (Fig. 4, B to E, and fig. S4, C, and D). In addition, we observed better homing of APL cells to the BM after prior co-culture

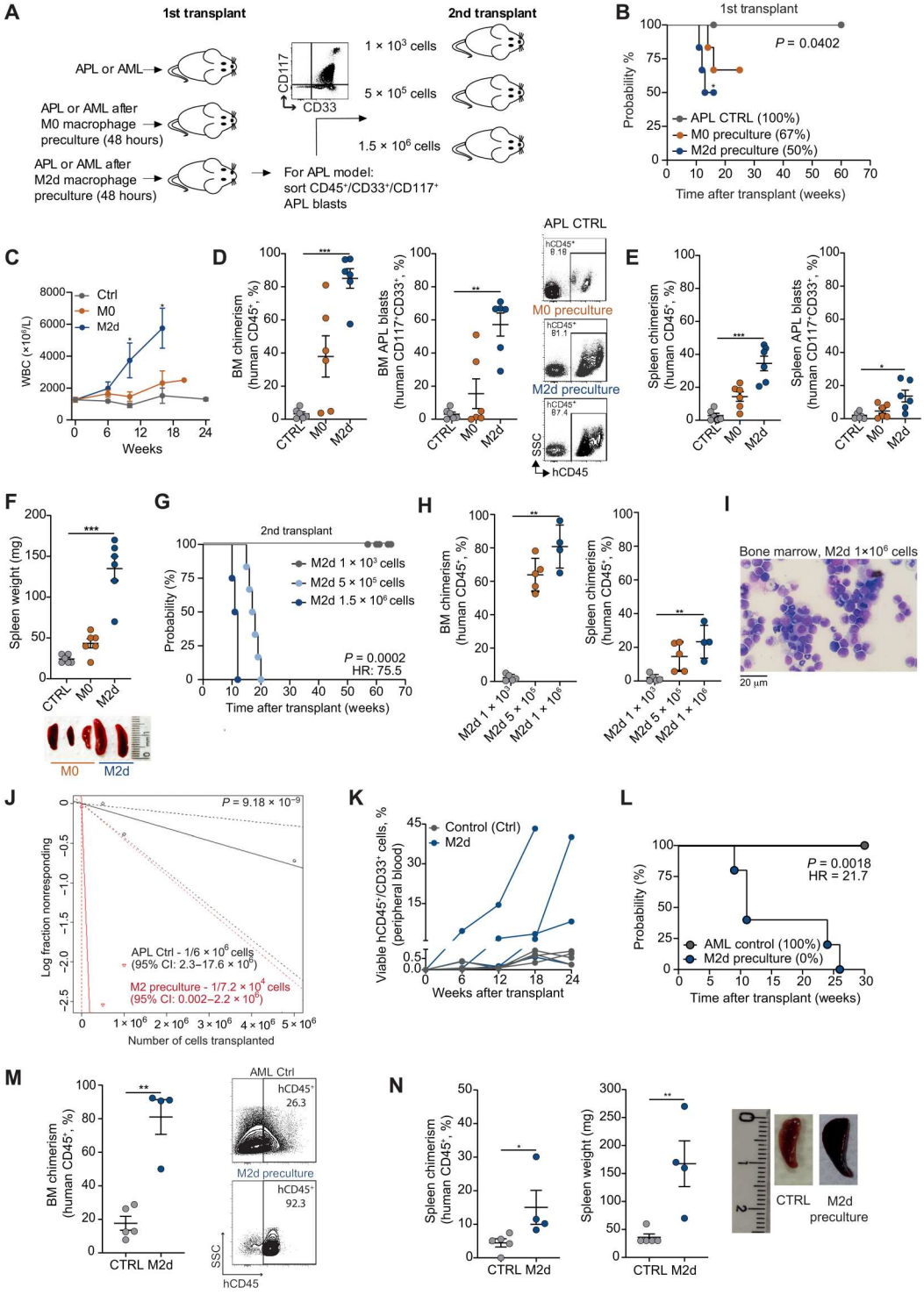

Fig. 4. Coculture of non-engrafting APL cells on M2 macrophages induces full-blown leukemia in a xenograft model. (**A**) Experimental in vivo setup. (**B**) OS of mice transplanted with primary APL blast transplanted without pre-culture or after preculture on M0/M2d macrophages for 48 hours. (**C** to **F**) Mice transplanted with APL blasts without pre-culture (Ctrl) or after preculture on M0/M2d macrophages were analyzed for WBC counts (C), for human $CD45^+CD117^+CD33^+$ chimerism (%) measured in the BM (D), for human $CD45^+CD117^+CD33^+$ chimerism (%) measured in the spleen (E), and spleen weight with representative spleen pictures (F). (**G**) OS of secondary transplanted mice receiving 1.5×10^6, 5×10^5, or 1×10^3 sorted human $CD33^+CD117^+$ APL blast cells from the primary transplant described in (B) to (F). (n = 3 to 6 per group). HR, hazard ratio. (**H**) Human $CD45^+$ chimerism levels (%) measured in the BM and spleen of secondary transplanted mice. (**I**) Representative cytospin of human APL blast cells retrieved from the murine BM. (**J**) In vivo Long-Term Culture-Initiating Cell (LTC-IC) analyses to determine LSC frequencies. 95% CI, 95% confidence interval. (**K**) Mice transplanted with AML blasts without pre-culture (Ctrl) or after preculture on M2d macrophages were analyzed for human $CD45^+CD33^+$ chimerism measured in the PB 6, 12, 18, and 24 weeks after transplant. (**L**) OS of mice transplanted with primary AML blast transplanted without pre-culture (control) or after preculture on M2d macrophages for 48 hours. (**M** and **N**) Mice transplanted with AML blasts without pre-culture (Ctrl) or after preculture on M2d macrophages were analyzed for human $CD45^+$ chimerism (%) measured in the BM (M), for human $CD45^+$ chimerism (%) measured in the spleen and spleen weight (N). (B, G, and L) Each dot represents an individual mouse, OS curves were estimated using the Kaplan-Meier method, and the log-rank test was used for comparison. (C and K) Two-way ANOVA. (D to F and H) Kruskal-Wallis test. (M and N) Wilcoxon signed rank test (two-sided). *P < 0.05, **P < 0.01, and ***P < 0.001.

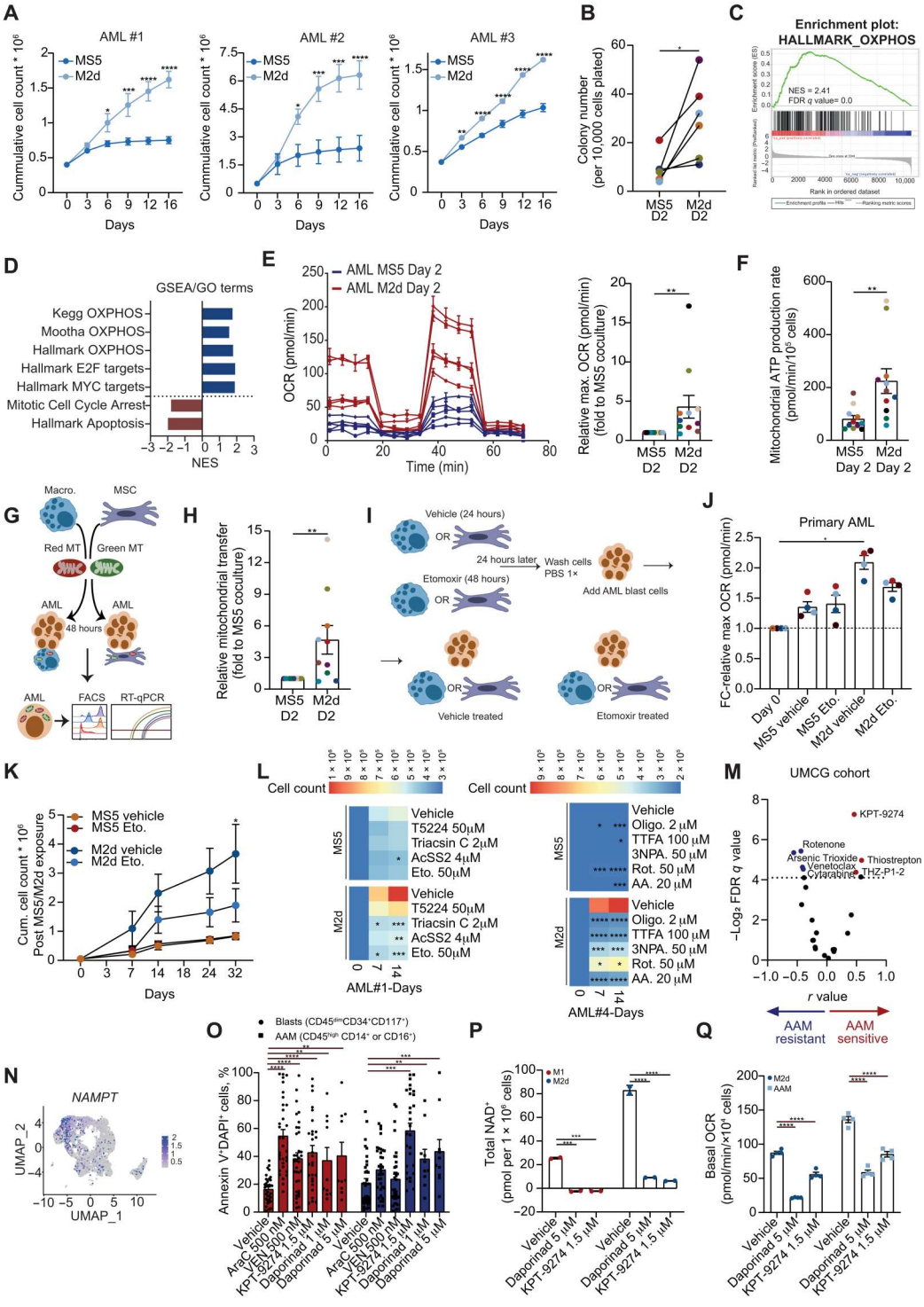

Fig. 5. M2-derived mitochondrial transfer promotes AML proliferation, which can be targeted. (**A**) Liquid cell proliferation of primary AML cells (technical duplicate/AML) and (**B**) CFU at day 14 of primary AML cells exposed to MS5/M2d macrophages (48 hours). (**C**) GSEA of the AML proteome with high versus low M2 macrophage (FACS). (**D**) GSEA/Gene Ontology (GO) analysis of the transcriptome (**E**) OCR/relative maximal OCR and (**F**) mitochondrial ATP production rate of primary AML cells exposed to MS5/M2d cells (48 hours). (**G**) Mitochondrial transfer (MTF) experimental scheme. (**H**) MTF measured in primary AML cells co-cultured on mitochondrial labeled MS5/M2d cells (48 hours). (**I**) Experimental scheme of AML cells co-cultured on etomoxir (Eto)–treated MS5/M2d cells. (**J**) OCR and (**K**) liquid proliferation of primary AML cells (three biological replicates) exposed to vehicle- or Eto (50 μM)–treated MS5/M2d cells (24 hours). (**L**) AML cells co-cultured on MS5/M2d cells treated with vehicle or drugs targeting FAO/mitochondrial ETC (24 hours) and then transferred to liquid culture after 48 hours. Heatmap displays AML liquid cell proliferation after exposure to treated MS5/M2d cells. (**M**) Pearson correlation of M2 macrophage levels (%) and ex vivo sensitivity in primary AML samples (n = 35). Blue and red dots indicate significant negative and positive correlations, respectively. (**N**) NAMPT expression in AAM. (**O**) Apoptosis (72 hours) induced in AML blasts and AAM after ex vivo treatment with Ara-C, VEN, KPT-9274 (n = 35), and Daporinad (n = 10). (**P**) Total NAD^+ levels in healthy M1/M2d macrophages treated with KPT-9274 or Daporinad. (**Q**) OCR of M2d macrophages/AAMs (n = 2) exposed to KPT-9274 or Daporinad. (B, E, F, H, J, O, and P) Each dot represents an individual patient. (A, K, L, P, and Q) Two-way ANOVA. (B, E, F, and H) Wilcoxon signed rank test (two-sided). (J) Friedman test. (O) Kruskal-Wallis test. (Q) Represents a technical duplicate. Data indicate the SEM. *P < 0.05, **P < 0.01, ***P < 0.001, and **** P < 0.0001.

on M2d macrophages compared to uncultured cells of the same patient (fig. S4E). These results were further confirmed in an in vitro transwell migration assay (fig. S4F). Concurrently, we detected enhanced surface expression of the integrin receptors CD49d (%) and an increase of the CD49d-f mean fluorescence intensity (MFI) upon M2d co-culture versus leukemic cells at diagnosis (fig. S4G).

Next, engrafted APL blasts ($hCD45^+CD117^+CD33^+$) from the primary PDX were sorted and used for secondary transplant (now without "training" on macrophages) in limiting dilution (1×10^3, 5×10^5, and 1.5×10^6 APL cells). After passage through primary mice, the cells retained self-renewal, and secondary transplanted mice developed full-blown APL when transplanted with 1.5×10^6 (median OS, 10 weeks) or 5×10^5 cells (median OS, 14 weeks)

(Fig. 4G). Mice transplanted with 1×10^3 cells only presented transient engraftment (Fig. 4, G and H, and fig. S4I). Engrafted mice presented symptoms of leukemia such as leukocytosis, anemia, and thrombocytopenia (fig. S4H). The BM from leukemic mice was highly infiltrated with human promyelocytes characterized by a high nuclear:cytoplasm ratio, visible nucleoli, and the presence of primary granules (Fig. 4I). Flow cytometry analysis confirmed that engrafted cells were predominantly $hCD117^+CD33^+$ (fig. S4J). Moreover, leukemic blast cells harvested from primary and secondary transplants presented with increased CD49d expression (fig. S4, K and L). Last, the LSC frequency for the control mice was $1/6.4 \times 10^6$, while trained APL cells displayed a frequency of $1/7.2 \times 10^4$ (Fig. 4J).

In line with our PDX models, we also evaluated the effect of macrophages on the transgenic *PML-RARA*$^+$ blasts from our syngeneic APL mouse model. Engraftment of $CD45.2^+$ *PML-RARA*$^+$ blasts was significantly enhanced after training when transplanted into sublethally irradiated $CD45.1^+$ recipients, with reduced median OS rates of 9.5 and 6.2 weeks for mice that received M0 and M2d pre-cultured cells, respectively, compared to 14 weeks for control mice (fig. S5A). The M2d-pre-cultured APL cells presented a more undifferentiated blast-like cell morphology compared to non-cultured APL blasts, which displayed a higher frequency of cells with cruller shaped nuclei post-sacrifice, characteristic for intermediate myeloid murine cells, which was confirmed by immunophenotypic analysis (fig. S5, B and C).

Last, we extended our analyses to other AML subtypes. We transplanted favorable AML subtypes such as AML samples with *NPM1* mutations and inv(16)(p13.1q22) after training on M2d-polarized macrophages ($n = 5$ independent samples; table S7). In all cases, pre-culturing on M2d macrophages strongly enhanced fatal leukemia development with high infiltration of leukemic blasts in the BM and spleen (Fig. 4, K to N). While low levels of engraftment were seen for the controls, human endpoints were not reached, and these animals were only euthanized at the endpoint of the experiment at 30 weeks (Fig. 4, L to N).

M2-derived mitochondrial transfer promotes AML proliferation, which can be targeted

While performing the co-culture of AML cells with M2 macrophages, we noticed that the non-phagocytosed remaining cells displayed increased cellular viability. Subsequent in vitro liquid culture of AML cells that were exposed to macrophages endowed AML cells with increased proliferative capacity compared to diagnosis and MS5 co-culture exposed cells, coinciding with enhanced colony-forming unit (CFU) capacity after M2 macrophage exposure (Fig. 5, A and B). Next, we compared the proteome of $CD34^+$- or $CD117^+$-sorted leukemic blasts (*2*) of patients that presented with a high versus low M2 macrophage content determined by flow cytometry. These analyses revealed that patients with AML harboring a high proportion of M2 macrophages in the BM had leukemic blasts of which the proteome was enriched for processes related to OXPHOS and "mitochondrial gene expression" (Fig. 5C). In line with these observations, RNA-seq analysis of AML blasts exposed to M2d macrophages or MS5 cells as a negative control confirmed that the process OXPHOS was up-regulated in the M2d-exposed blast cells (Fig. 5D, fig. S5D, and tables S8 to 11). Functionally, we observed increased oxygen consumption rates (OCR) and extracellular acidification rates (ECAR) (Fig. 5E and fig. S5E) and mitochondrial adenosine triphosphate (ATP) production (Fig. 5F) after a 2-day coculture of leukemic blasts ($n = 11$) on M2d macrophages, which was much less pronounced after coculture on MS5 stromal cells. Concomitantly, we noticed decreased glucose consumption and lactate production rate by leukemic cells exposed to M2d macrophages compared to MS5 cells (fig. S5F).

The increase in OCR suggested enhanced mitochondrial metabolism, which prompted us to determine whether macrophages could transfer mitochondria to primary AML cells (Fig. 5G). Primary AML cells were cocultured for 48 hours on mitochondria-labeled M2d macrophages or MS5 cells. Flow cytometry analysis revealed an efficient mitochondrial transfer from M2d macrophages to leukemic blasts, which was superior when compared to mitochondrial exchange from MS5 control (Fig. 5H). Real-time quantitative polymerase chain reaction (qRT-PCR) evaluation of the murine mitochondrial DNA content from murine macrophages and MS5 cells confirmed mitochondrial transfer, which could be detected in blast cells up to 7 days after co-culture (fig. S5G).

FA oxidation (FAO) is one of the main mechanisms used by macrophages to fuel the Krebs cycle, culminating in M2 polarization (*31*). To evaluate whether FAO is the driver of OXPHOS in M2d-exposed AML cells, we treated M2d macrophages with the FAO inhibitor etomoxir (Eto) for 24 hours. After 24 hours, macrophages were washed and co-cultured with primary AML cells for 24 hours to measure their functional respiration (Fig. 5I). Eto-treated M2d macrophages exhibited decreased OCR (fig. S5H). The increase in OCR in primary AML cells after co-culture on M2d macrophages was much less pronounced when macrophages were pretreated with Eto (Fig. 5J). In line with this, the enhanced growth capacity of primary AML cells in liquid cultures after co-culture on M2d macrophages that we observed before (Fig. 5A) was strongly reduced when macrophages were pre-treated with Eto (Fig. 5K). To independently confirm a role for FAO and the tricarboxylic acid cycle, we extended the panel of inhibitors, and these studies further supported the notion that disruption of mitochondrial energy production in M2 macrophages compromises their capacity to support AML blasts (Fig. 5L and fig. S5I). Overall, these data suggest that the metabolic changes induced by macrophages are, at least in part, mediated via mitochondrial transfer and can promote the proliferation of leukemic cells.

Last, given the importance of M2 macrophages in supporting leukemia progression, we questioned whether we could identify compounds directed against these tumor-supportive cells. An ex vivo drug screen was set up in which 35 primary AML samples were treated with different chemotherapeutic and metabolism-related drugs. We specifically initiated screens with mononuclear cell fractions to be able to evaluate the efficacy of these compounds on the leukemic blasts as well as on the tumor-supportive AAMs. First, we identified that patients with a high percentage of AAMs exhibited increased resistance to Cytarabine (AraC) and venetoclax (VEN) and increased sensitivity to some macrophage-targeting drugs such as thiostrepton (*32*) and KPT-9274 (Fig. 5M). KPT-9274 inhibits the nicotinamide adenine dinucleotide (NAD^+) salvage pathway gene nicotinamide phosphoribosyltransferase (*NAMPT*), which we identified to be up-regulated in AAMs (Fig. 5N and fig. S5J). NAMPT inhibition was recently also identified as a metabolic vulnerability in LSCs by disrupting lipid homeostasis (*33*). We observed that both leukemic blasts and AAMs

showed strong sensitivity to NAMPT inhibition, in contrast to, e.g., AraC and VEN, which induced apoptosis of leukemic blasts in some patients but not in the tumor-supportive AAMs (Fig. 5O). Multivariate analysis identified the presence of *FLT3*-ITD mutations as an independent confounding factor predicting higher sensitivity to NAMPT inhibition ($P = 0.034$). Furthermore, treatment of M2 macrophages or AAMs with NAMPT inhibitors (KPT-9274 and Daporinad) resulted in a strong decrease in total NAD^+ levels (Fig. 5P) and mitochondrial respiration (Fig. 5Q and fig. S5K). Together, our study outlines the clinical relevance and functional importance of tumor-supportive macrophages, and we provide alternatives for effective targeting strategies aimed at the tumor microenvironment.

DISCUSSION

Cancer progression is dictated not only by the intrinsic alterations acquired by cancer cells but also by the microenvironment in which malignant cells reside. Being an essential part of the tumor microenvironment of solid tumors, tumor-associated macrophages are often associated with poor prognosis due to their pro-tumorigenic functions promoting proliferation, dissemination, and immune evasion of cancer cells (*34*). In AML, we find strong heterogeneity in the macrophage landscape, which is more tumor-suppressive and M1 polarized in some patients yet more tumor-supportive and M2 polarized in others, strongly correlating with survival. In contrast to solid tumors, AML-derived macrophages can share the same cell of origin as the leukemic clones themselves [(*35*) and our study], indicating that macrophages are not always necessarily wild type. We find that the phagocytic capacity of AAMs is reduced compared to normal macrophages, and also the introduction of mutations such as the *FLT3*-ITD or KD of *DNMT3A* in CB-derived macrophages can impair phagocytosis, although more experiments are required to further substantiate these findings and uncover underlying mechanisms. scGSEA on AAMs identified clear transcriptome differences associated with an M2 macrophage signature and immunosuppression in a subgroup of patients. Recent studies have shown that clonal hematopoiesis of indeterminate potential (CHIP) associated mutations like *TET2*, *ASXL1*, and *DNMT3A* detected in myeloid cells and macrophages were shown to drive a pro-inflammatory phenotype contributing to the expansion of mutant HSC clones and bone remodeling in the BM (*36*–*38*). Another study conducted in intestinal tumors observed that the deletion of *TP53* in macrophages increased the incidence of intestinal tumor development (*39*). In colon cancer, gain-of-function *TP53* mutations resulted in the generation of miR-1246–containing exosomes that were taken up by macrophages and reprogrammed them into a tumor-promoting state (*40*). Mutations in the *TP53* gene are detected in 8 to 20% of patients with AML and MDS, respectively, and predict poor clinical outcomes (*41*). Here, we show that AML-derived macrophages exhibit decreased phagocytic activity, which is in part caused by the acquisition of AML mutations thereby potentially facilitating leukemia progression.

In vivo intra-BM, coinjection of M2d macrophages allowed the induction of full-blown leukemia, while APL blasts without co-injected macrophages were unable to expand in NSGS mice. The leukemic burden was consistently superior in M2d-injected bones compared to M0 bones, suggesting that, in particular, M2d-type macrophages provide the leukemia-propagating signals. At first, these results were rather unexpected as previous studies would suggest that phagocytosis of murine resident macrophages, including those from immunodeficient mice, would obstruct rather than promote engraftment of pluripotent embryonic stem cells and murine (MEIS1/HOXA9 and MN1-driven) AML cells (*42*, *43*). We also observe that macrophages isolated from immunodeficient NSG mice have phagocytic activity against leukemic cells. We hypothesize that these macrophages in healthy mice are polarized to a tumor-suppressive M1 phenotype, in line with what we observe for macrophages isolated from healthy human donors, but that tumors cells can reprogram macrophages into tumor-supportive M2 subtypes to support their growth or that mutant macrophages that descend from tumor clones directly display impaired phagocytosis. It has been observed that AMLs, in part via their secretome, can repolarize tumor-suppressive M1 macrophages into tumor-supportive M2 macrophages (*44*). Upon transplantation into an intrinsically tumor-suppressive macrophage environment, leukemic cells will need to overcome this first barrier.

Intriguingly, a 2-day in vitro exposure of APL and favorable AML blasts to M2 macrophages—which we refer to as training—allowed efficient engraftment followed by fatal leukemia in NSGS mice. In vitro, the fate of leukemic blasts when encountering M2 macrophages can be twofold: either they are phagocytosed or they are altered in such a way that their leukemic potential has increased. Chao *et al.* (*45*) showed that the process of programmed cell removal relies on an equilibrium of pro- and anti-phagocytic signals, whereby cancer cells tend to up-regulate the expression of "Don't eat me" signals such as CD47 to evade the innate immune system and facilitate tumor growth (*23*). As a result, the blockage of CD47 has been shown to delay tumor growth by increasing the phagocytic activity of macrophages (clinical trial identifier: NCT05079230). Analysis of RNA-seq data on mononuclear AML samples of the TCGA-AML and BeatAML cohorts indicated that the expression of *CD47* was overall homogeneous, whereby the highest expression was detected in poor-risk cytogenetic abnormalities and CBFB-MYH11 patients. CD47 expression on leukemic blasts also did not change after 2-day training on M2d cells. In contrast, the expression of *CALR*, a well-described "eat me signal," presented more heterogeneity with the highest expression detected in APL and CBF leukemia patients known to be favorable AML subtypes. Also, CALR expression was reduced on blasts after exposure to M2d macrophages. CALR is a multifunctional protein that acts as a chaperone in the endoplasmic reticulum, regulates Ca^{2+} homeostasis, and can be translocated to the surface to stimulate phagocytic uptake by the immune system (*46*). In solid tumors and lymphomas, low levels of CALR were associated with poor clinical outcomes due to poor anticancer immunity (*45*, *47*). In our analysis, $CALR^{low}$ patients were associated with a stem-like phenotype and displayed high expression of genes like *GPR56*, *MEIS1*, and *HOXA9* linked to stemness and poor prognosis. Upon M2 coculture, we observed a decrease in *CALR* expression, suggesting that M2 macrophages could induce transcriptional changes related to stemness. In addition, low levels of *CALR* would also suggest a decreased availability of CALR to be translocated to the surface facilitating leukemia immune evasion from the innate immune system in a xenograft transplant setting. Our data suggest that leukemic cells harvested post-macrophage co-culture comprehend a higher frequency of cells enriched for stemness signatures that are equipped to evade macrophages in PDX models while also

highlighting the previously overlooked importance of macrophages in the engraftment of primary AML samples. Last, we also observe that the pre-culture on M2 macrophages can increase the expression of integrins, which play an essential role during HSC homing and engraftment (*48*). Studies in which CD49d was either deleted or blocked demonstrated decreased homing and engraftment of HSPCs, even when $CD34^+$ cells were directly injected into the BM (*48*, *49*). In line with this notion, we demonstrate that M2d-exposed primary APL cells acquire improved homing capacities in vivo, and it is conceivable that the up-regulation of integrins further facilitates APL engraftment and leukemogenesis.

While our data show that conditioned medium of M2d macrophages can improve primary AML cell growth, these effects were less prominent compared to direct cell-to-cell contact of AML blasts with macrophages. A study published by Hur *et al.* (*12*) indicated that LT-HSC quiescence is facilitated by the cross-talk of CD82 expressed by LT-HSC interacting with $DARC^+$ macrophages. Recently, Wattrus *et al.* (*50*) showed that the depletion of macrophages significantly decreased the number of HSC clones using the brainbow zebrafish model. The authors identified HSCs that expressed Calr/3a/3b which interacted with Lrp1ab on macrophages. As a result, some of the HSCs were completely engulfed, while in other HSCs, cell cycle progression was induced (*50*) very similar to our observations with macrophage-leukemic blast interactions. We find that one of the consequences of direct interactions of leukemic blasts with macrophages is the transfer of mitochondria, thereby driving OXPHOS metabolism in AML cells, which was also reported for interactions with MSCs (*51*). This might well underlie the increased fitness of leukemic blasts we observe after training on M2d macrophages, resulting in increased clonogenic capacity, enhanced proliferation in liquid cultures, and improved in vivo leukemogenesis. These data corroborate with a previous study, which demonstrated that the co-culture of human CB $CD34^+$ on M2 macrophages significantly increased the number of $CD34^+$ and LT-HSCs (*52*). Although further studies are required, it is quite conceivable that the formation of nanotubes, initiated via the exosome complex, facilitates mitochondrial hijacking between AML blasts and macrophages, in line with a previous study (*53*). Furthermore, it is possible that other factors such as plasma membrane marker or RNA are exchanged between AML blasts and macrophages, which needs to be investigated in future studies.

Our insights into the macrophage landscape in patients with AML not only provide improved diagnostic tools for patient stratification based on the presence or absence of a tumor-supportive immune microenvironment but also provide alternative means for targeting strategies, not directed at the blasts per se but rather at their microenvironment. Our data indicate that the 2-day coculture of primary AML cells on M2d macrophages is sufficient to induce LT effects on AML proliferation, which could be abrogated by the pretreatment of macrophages with several compounds targeting FAO or mitochondrial respiration, including the carnitine palmitoyltransferase 1A (CPT1A) inhibitor Eto, thereby inhibiting FA-driven OXPHOS. Overall, it is conceivable that the metabolic changes increase the proliferation capacity of leukemic cells resulting in a more aggressive leukemia. Notably, our single-cell analysis focusing on the AAMs revealed that these cells rely on FAO and NAD^+ generation to support their metabolic needs. Therefore, therapeutical strategies targeting those pathways could be clinically interesting for AML patients with high M2 profiles, representing a dual strategy of targeting the tumor cells and the tumor microenvironment, reducing the chances of a future niche-supported relapse events.

Together, our study indicates that interactions between leukemic blasts and macrophages can have a profound impact on tumor cell biology, in part mediated via direct interactions and the exchange of organelles such as mitochondria and in part also via genetic alterations found in AAMs (summarized in fig. S6). Our insights provide improved tools for patient stratification and allow for alternative treatment strategies aimed at targeting the tumor microenvironment.

MATERIALS AND METHODS

Study approval and animal welfare

BM samples of patients with APL used in for in vivo experiments were studied after informed consent and protocol approval by the Ethical Committee in accordance with the Declaration of Helsinki (registry #12920; process number #13496/2005; CAAE: 155.0.004.000-05 and CAAE: 819878.5.1001.5440). Mononuclear cells (MNCs) were isolated via Ficoll (Sigma-Aldrich) separation and cryopreserved. PB and BM samples of patients with AML were studied after informed consent and protocol approval by the Medical Ethical Committee of the University Medical Centre Groningen (UMCG) in accordance with the Declaration of Helsinki. An overview of patient characteristics can be found in Table 1.

For the in vivo experiments, all animals were housed under specific pathogen–free conditions in individually ventilated cages during the whole experiment. The animals were maintained according to the Guide for Care and Use of Laboratory Animals of the National Research Council, USA, and to the National Council of Animal Experiment Control recommendations. All experiments were approved by the Animal Ethics Committee of the University of São Paulo (protocols #176/2015 and #095/2018).

Human sample collection and patient information

MNCs from patients with AML/APL were isolated via Ficoll (Sigma-Aldrich) separation and cryopreserved. PB and BM samples of patients with AML were studied after informed consent and protocol approval by the Medical Ethical Committee of the UMCG in accordance with the Declaration of Helsinki. Neonatal CB was obtained from healthy full-term pregnancies from the Obstetrics Departments of the University Medical Center and Martini Hospital in Groningen, The Netherlands, after informed consent. The protocol was approved by the Medical Ethical Committee of the UMCG. Donors are informed about procedures and studies performed with CB by an information sheet that is read and signed by the donor, in line with regulations of the Medical Ethical Committee of the UMCG (protocol #NL43844.042.13). PB mononuclear cell–derived $CD34^+$ stem cells (PBMSCs) and CB-derived $CD34^+$ cells were isolated by density gradient separation, followed by a hematopoietic progenitor magnetic associated cell sorting kit from Miltenyi Biotech (#130-046-702) according to the manufacturer's instructions. All $CD34^+$ healthy cells were prestimulated for 24 to 48 hours before experimental use. CB-derived cells were prestimulated with Stemline II hematopoietic medium (Sigma-Aldrich, #S0192), 1% penicillin/streptomycin (PS) supplemented with stem cell factor (SCF; 255-SC, Novus Biologicals), FLT3 ligand (Amgen), and N-plate (TPO) (Amgen) (all 100 ng/ml).

PBMSC CD34$^+$ cells were prestimulated with Stemline II, 1% PS, 20% fetal calf serum (FCS) along with SCF, FLT3 ligand, N-plate (all 100 ng/ml), and IL-3 (Sandoz) and IL-6 (both 20 ng/ml). Primary AMLs were grown on MS5 stromal cells with granulocyte colony-stimulating factor (G-CSF; Amgen), N-Plate, and IL-3 (all 20 ng/ml).

Cell lines

All cell cultures were maintained in a humidified atmosphere at 37°C with 5% CO_2. Mycoplasma contamination was routinely tested. All leukemia cell lines were authenticated by short tandem repeat analysis. The HS27A (CRL-2496) and HL60 (CCL-240) cell lines were obtained from the American Type Culture Collection and grown in Dulbecco's modified Eagle's medium (DMEM; for HS27A; Gibco, USA) or RPMI (for HL60; Gibco, USA) with 10% FCS. The MOLM13 (ACC 554) cell line was obtained from the DSMZ-German Collection of Microorganisms and Cell Cultures. AraC, rotenone (Rot), 3-nitropropionic acid, 2-thenoyltrifluoroacetone, antimycin A (AA), and oligomycin A were obtained from Sigma-Aldrich (St. Louis, USA). VEN and the NAMPT inhibitor KPT-9274 were obtained from Selleckchem (Houston, USA). Eto, triacsin C, T-5224, Acetyl coenzyme A (Ac-CoA) synthase inhibitor1 (AcSS2), and (E)-Daporinad were obtained from MedChemExpress (Groningen, NL).

Single-cell analysis

The scRNA-seq dataset of AML BM cells and HD BM cells were obtained from the Gene Expression Omnibus (GEO) database (GSE116256). Information about AML cells used and cell preparation was retrieved from van Galen *et al.* (*18*). Data had already been quality filtered using the parameters number of unique molecular identifiers (UMIs) per cell > 1000, number of genes per cell > 500, and mitochondrial genes percentage < 5% (total = 21,173 cells). Using the SEURAT 4.0.1 package (*54*), we used fast integration by reciprocal principal components analysis in 12 diagnosis AML and 3 HD single-cell datasets. Thus, 19 distinct clusters were identified (fig. S1, A and B). Next, we isolated single cells that presented enrichment for macrophage gene expression markers (*55*), which we then defined as AAMs. Thus, 5 of the 19 clusters were identified to be enriched for macrophage signatures. These obtained AAM clusters were then projected in a UMAP [fig. S1, A and B, clusters (K) 0, 3, 8, 10, and 14: in total, 7030 cells were identified from nine AML samples and two healthy BM donors, due to low frequency of monocytic cells in the other samples]. These AAM cells were reintegrated, reclustered, and UMAP reduced (Fig 1B). For single-cell gene set enrichment, we used the SCENIC AUCell package (*56*). Briefly, we computed the area under the curve (AUC) per cell for each gene set (table S6) and used it to plot onto our UMAP reductions or to compute the density plot AML versus HD (Fig. 1, F and G).

Flow cytometry

Cryopreserved MNC fractions of AML/APL patients were thawed, resuspended in newborn calf serum supplemented with deoxyribonuclease I (20 U/ml), 4 μM $MgSO_4$, and heparin (5 U/ml), and incubated at 37°C for 15 min. To analyze the myeloid fraction of the AML/APL bulk sample, 5×10^5 mononuclear cells were blocked with human FcR blocking reagent (Miltenyi Biotec) for 5 min and stained with the following antibodies: CD45–fluorescein isothiocyanate (FITC), HLA-DR-phycoerythrin (PE), CD14-PerCP, CD16-APC-Cy7, CD163-PE-Cy7, CD206-Brilliant Violet 421 (BV421), CD36-PE-Cy7 (in a separate tube), and CD80-APC for 20 min at 4°C. A more mature myeloid population was detected on the basis of the CD45 staining, and inside this gate, HLA-DR–positive cells were selected to analyze the CD14 versus CD16 cellular distribution. The different CD14-CD16 populations (CD14$^+$-CD16$^-$; CD14$^+$-CD16$^+$; CD14$^-$-CD16$^+$) were then analyzed for their expression of the M1 marker CD80 and the M2 markers CD36, CD163, and CD206. Fluorescence was measured on the BD LSRII or FACS CantoII and analyzed using FlowJo (Tree Star Inc.). For each sample, a minimum of 5000 events were acquired inside the SSC-A^{high} CD45^{high} HLA-DR$^+$ population.

Mutational analysis in AAM

Cryopreserved MNC fractions of patients with AML/APL were thawed as described in the "Flow cytometry" section. To sort AAM and blast cells from AML bulk samples, 1×10^7 mononuclear were blocked with human FcR blocking reagent (Miltenyi Biotec) for 5 min and stained with the following antibodies: CD45-FITC, HLA-DR-PE, CD14-PerCP, and CD163-Pe-Cy7 for 20 min at 4°C. Cells were then washed and filtered in a 70-μm cell filter to generate single cells. Cells were sorted using the SH800S Sony cell sorter (Sony Biotechnology, NL). The more immature AML blast population (CD45^{dim}/CD14$^-$/HLA-DR$^-$/CD163^{dim}) and the AAM population (CD45^{high}/CD14$^+$/HLA-DR$^+$/CD163$^+$) were sorted in separate tubes and stored for DNA extraction. For molecular analysis, genomic DNA was extracted using the Puregene kit (Gentra System) according to the manufacturer's protocol. Standard polymerase chain reaction and sequencing techniques were performed for the detection of *NPM1* and *FLT3*-ITD mutations.

Immunohistochemistry

Tissue sections were cut from formalin fixed embedded BM biopsies of patients with AML at diagnosis. CD68 and CD163 were stain-visualized by the Ventana Benchmark Ultra automated slide stainer, after antigen retrieval (Ultra CC1, Ventana Medical Systems), using monoclonal antibodies CD68 (1:100; PG-M1, Dako) and CD163 (MRQ-26, ready to use, Ventana) and Ultraview (Ventana). Digital images of these slides were scored for percentage of positively staining BM cells.

Clinical endpoint analysis

Survival analyzes were performed in AML patients treated with intensive chemotherapy (3 + 7 scheme) as an induction protocol (*57*). First, we calculated the FC values of patients with AML, comparing the levels of M1 (CD80) and M2 (CD163 and CD206) macrophage markers in the myeloid mature compartment (defined by SSC^{high}CD45^{high}HLA-DR$^+$) with the HDs. Next, we performed a nonsupervised clustering analysis (Euclidian complete linkage) of the patients with AML, based on the FC for M1 and M2 markers, and dichotomized patients into AAM^{low} and AAM^{high} groups. OS was defined as the time from diagnosis to death from any cause related to the disease; those alive or lost to follow-up were censored at the date last known alive. For patients who achieved complete remission (CR), disease-free survival (DFS) was defined as the time from CR achievement to the first adverse event: relapse, development of secondary malignancy, or death from any cause, whichever occurred first. For the MDS cohort (GSE58831), the PFS was

defined as the time after treatment starts until progression to AML or death from any cause. Univariate and multivariate proportional hazards regression analysis was performed for potential prognostic factors for OS. Potential prognostic factors examined and included in multivariable regression analysis were ELN2010/2017 (when available, BeatAML cohort) risk stratification, age at diagnosis (analyzed as continuous variable), gender, and our proposed clustering regarding the macrophage content. Proportional hazard (PH) assumption for each continuous variable of interest was tested. Linearity assumption for all continuous variables was examined in logistic and PH models using restricted cubic spline estimates of the relationship between the continuous variable and log relative hazard/risk. Descriptive analyses were performed for patient baseline features. Fisher′s exact test or chi-square test, as appropriate, was used to compare categorical variables. Mann-Whitney or Kruskal-Wallis test was used to compare continuous variables. Details of the statistical analysis and clinical endpoints were described elsewhere. All *P* values were two-sided with a significance level of 0.05. All statistical analyses were performed using the statistical package for the social sciences (SPSS) 19.0 and R 3.3.2 (The CRAN project, www.r-project.org) software.

Development of a M2 signature suitable for patients with AML

The genetic signatures from M1 and M2 macrophages were retrieved from the FANTON, HPCA, BluePrint, and CIBERSORT signatures (*58*–*60*). Genes with unique differential expression in M2 but not M1 macrophages were selected for survival analysis using AML cohorts (fig. S1D). The gene expression of the two M2 macrophage markers used in our flow cytometry panel (CD163 and MRC1-CD206) and the expression of the M2 genes *FGR*, *CD52*, *RASA3*, and *GSK1B* were able to predict poor OS in at least two independent cohorts (fig. S1F). Out of those genes, *CD163*, *RASA3*, *FGR*, and *GSK1B* exhibited increased expression in the $CD34^-$ cells, when compared to the $CD34^+$ cells in AML BMs. Next, using the TCGA cohort (*21*), patients were dichotomized as a low or high expression using receiving operating characteristics curve and the C index and were interrogated for univariate and multivariate Cox proportional hazards model regression analyses for OS. Including age, sex, and European LeukemiaNet (ELN2010) as cofounders, we identified the independent prognostic predictors by backward elimination using an exclusion significance level of 5%. The M2-AAM signature was defined as the weighted sums of hazard ratio from the final Cox model from independent prognostic genes (*CD163*, *MRC1*, *FGR*, *CD52*, *RASA3*, and *GSK1B*). Internal validation was performed using a nonparametric bootstrap procedure with 1000 resamplings to get estimates of HR between risk categories corrected for overfitting. We used the MDS cohort (GSE58831) to validate our M2-AAM signature.

Real-time quantitative polymerase chain reaction

For quantitative RT-PCR, RNA was reverse-transcribed using the iScript cDNA synthesis kit (Bio-Rad) and amplified using SsoAdvanced SYBR Green Supermix (Bio-Rad) on a CFX384 Touch Real-Time PCR Detection System (Bio-Rad). The ACTB, HPRT1, and RPL30 were used as housekeeping genes. Primer sequences are listed in the key resources table.

Human macrophage generation

MNCs were isolated by a density gradient using Ficoll (Sigma-Aldrich) from HDs or allogeneic donors. Next, 2.5×10^6 or 5×10^6 mononuclear cells were seeded into 12- or 6-well plates and incubated for 3 hours at 37°C in RPMI medium supplemented with 10% FCS, 10% heat-inactivated and filtered human serum (AB serum, Thermo Fisher Scientific), and 1% PS. After 2 hours of incubation, the nonadherent cell fraction was removed, and the new RPMI medium supplemented with 10% FCS, 10% human serum, and 1% PS was added. In addition, GM-CSF (50 ng/ml; Prepotech) or M-CSF (Prepotech/Immunotools) growth factors were added to the medium to generate pre-orientated M1 and M2 macrophages, respectively. Monocytes were differentiated into macrophages over a time span of 6 days, and at day 3, half of the medium was renewed.

Murine macrophage generation

Mice were anesthetized with an overdose of ketamine/xylazine solution and euthanatized by cervical dislocation to collect femur and tibia. Next, the epiphyses were cut off and a syringe of 25 G filled with PBS (1% FCS) was used to flush the BM onto a 70-μm cell strainer placed on a 50-ml tube. Red blood cells were lysed for 10 min at 4°C and washed with PBS. Three million BM mononuclear cells were seeded in a 100 by 20 mm petri dish and cultured in RPMI medium supplemented with 10% FCS, 15% of L929 supernatant, and 1% PS for 7 days. At day 3, half of the medium was renewed.

Macrophage polarization

At day 6, human macrophages were washed with phosphate-buffered saline (PBS), and new RPMI medium supplemented with 10% FCS was added. GM-CSF–cultured macrophages were polarized to M1 macrophages with interferon-γ (20 ng/ml; Prepotech) and lipopolysaccharide (100 ng/ml; Sigma-Aldrich), while M-CSF cultured macrophages were polarized to M2d macrophages with M-CSF (10 ng/ml) and IL-6 or M2a (20 ng/ml) with M-CSF (10 ng/ml) and IL-4 (20 ng/ml; Prepotech). To generate M0 macrophages, M-CSF–cultured macrophages were kept with M-CSF (50 ng/ml) in the medium.

Likewise, murine macrophages were washed with PBS and new RPMI medium supplemented with 10% FCS and 1% PS was added at day 6. To polarize murine macrophages to M2d macrophages, IL-6 (20 ng/ml; Prepotech) was added to the medium. M0 macrophages were generated by maintaining the cells in 15% of the L929 supernatant.

FACS staining of macrophages

After polarization, macrophages are detached with TrypLE (Thermo Fisher Scientific) according to the manufacturer′s instructions. A total of 1×10^5 cells were washed in PBS and resuspended in PBS (2 mM EDTA, 2% BSA, and 0.02% NaN3) and 10 μl of FcR blocking reagent. Macrophages were incubated 30 min at 4°C. Fluorescence was measured on the BD LSRII or FACS CantoII and analyzed using FlowJo (Tree Star Inc.). For each sample, a minimum of 10,000 viable cells [4′,6-diamidino-2-phenylindole (DAPI)–negative events] were acquired.

In vitro primary AML cell proliferation on macrophages

Cryopreserved MNC fractions of patients with AML were thawed as described in the "Flow cytometry" section. $CD34^+$ cells were

isolated from primary AML patients on the autoMACS using a magnetically activated cell sorting progenitor kit (Miltenyi Biotech). In case of *NPM1*-mutated AMLs with CD34 expression <1% and APL samples, the $CD117^+$ blast cells were isolated.

A total of 2×10^5 to1×10^6 primary AMLs were cultured on distinct macrophage subtypes and on MS-5 as a control for 10 days. MS-5 cells were plated on gelatin-coated culture flasks and expanded to form a confluent layer (above 70% of confluence). The cocultures were performed in Gartner's medium consisting of alpha-MEM (Thermo Fisher Scientific) supplemented with 12.5% FCS (Gibco), 12.5% horse serum (Gibco), 1% PS, 2 mM glutamine (Gibco), 57.2 mM β-mercaptoethanol (Merck Sharp & Dohme BV), G-CSF (20 ng/ml), N-plate (TPO), and IL-3. Co-cultures were grown at 37°C and 5% CO_2 and demi-populated after counting if necessary. Cell proliferation was assessed until 10 to 14 days of coculture with a hemocytometer and cross-validated by counting the viable $DAPI^-$ $CD45^{dim}$ cell population by flow cytometry using the NovoCyte Quanteon System (Agilent, CA, USA).

Generation of conditioned medium and in vitro primary AML culture

Conditioned medium was collected 24 hours after macrophage polarization as and stored at −80°C until usage. Conditioned medium was only used once after thawing. MS-5 cells were seeded in a gelatin-coated 12-well plate and expanded to form a confluent layer. Next, 2.5×10^5 primary AML cells were added to the MS-5 cells and cultured in 750 μl of Gartner's medium and 750 μl of either M1 or M2d macrophage polarization medium. The cytokines G-CSF, N-plate (TPO), and IL-3 were added at a concentration of 20 ng/ml. Co-cultures were grown at 37°C and 5% CO_2 and demi-populated after counting if necessary. Cell proliferation was assessed with a hemocytometer for 10 days.

CFU assay

Primary $CD3^+$ depleted AML cells (1×10^6) were put in coculture with either macrophages or MS-5 cells for 48 hours. The cocultures were performed in Gartner's medium. After 48 hours, cells were collected, washed, and counted. A total of 1×10^4 AML cells after co-culture were plated in semisolid methylcellulose medium supplemented with human cytokines MethoCult H4435 (StemCell). Colonies were detected after 14 days and scored. For CFU experiments to determine the clonogenic potential of $CALR^{high}$ and $CALR^{low}$ AML cells, the top 1% highest and lowest CALR-expressing cells were sorted, and a total of 1×10^4 sorted cells were plated in semisolid methycellulose medium, as described above.

In vivo intra-BM APL PDX model

Macrophages were detached with TrypLE and washed two times with PBS at 450*g*. Macrophages were stained with DAPI, HLA-DR, and CD206 to confirm viability and the macrophage subtype. Macrophages were resuspended in PBS at a working concentration of 1×10^5/10 μl. Eight- to 10-week-old female NSGS (*NOD.Cg-Prkdcscid Il2rgtm1Wjl Tg(CMV-IL3,CSF2,KITLG)1Eav/MloySzJ*) mice were anesthetized, and tramadol (25 mg/kg) was injected subcutaneously. The intratibial injection of macrophages was performed according to the percutaneous approach (*61*). In summary, under anesthesia through a nose cone, the mouse was placed in a supine position, and the pre-shaved knee was cleaned with 70% ethanol and maintained in a flexed position. A 30-G needle was placed percutaneously through the knee joint and inserted by rotating the syringe. Once the BM space was reached, 10 μl of the BM was aspirated (to free BM space). Next, 10 μl of macrophages corresponding to 100,000 cells in total were injected into the BM with a new needle. M0 macrophages were injected into the left tibia, while M2d macrophages were injected into the right tibia. Control mice received 10 μl of PBS. On the next day, five different cryopreserved MNC fractions of APL patient samples were thawed and depleted for $CD3^+$ cells. Next, 1×10^6 primary APL cells were injected via the retro-orbital sinus into macrophage recipient and control mice. Human $CD45^+$ levels were measured regularly in blood obtained by submandibular bleeding. Twelve weeks post-transplant mice were euthanized, and each leg of the macrophage recipient mice was processed separately. Cells from BM, spleen, and spine were collected and stained for human CD45, CD11b, HLA-DR, CD33, and CD117 to detect human APL blast cells ($CD45^+CD33^+CD117^+CD11b^-HLA\text{-}DR^-$ cells). All specimens were acquired by flow cytometry (FACS CantoII) and analyzed with the FlowJo software (Treestar Inc., USA). For each sample, a minimum of 20,000 viable events were acquired. In addition, cytospin preparations stained with May-Grünwald-Giemsa were used to evaluate the morphology of human APL blasts.

In vivo preculture AML/APL PDX model

Human macrophages were generated and polarized as described in the "Human macrophage generation," "Murine macrophage generation," and "Macrophage polarization" sections in six-well plates. AML and APL patient samples were thawed as described in the "Flow cytometry" section (clinical characteristics in table S7) and depleted for $CD3^+$ cells. In total, 5×10^6 blast cells were put in co-culture per well for 48 hours. The co-cultures were performed in Gartner's medium. After 48 hours, suspension cells were collected and washed two times with PBS. Primary AML/APL blast cells were counted, and 1×10^5 blast cells exposed to macrophages were set aside to evaluate the purity of these cells to ensure no macrophage contamination. Next, 1.5×10^5 tumor cells were injected via the retro-orbital sinus into 8- to 10-week-old female NSGS (*NOD.Cg-Prkdcscid Il2rgtm1Wjl Tg(CMV-IL3,CSF2,KITLG)1Eav/MloySzJ*) mice. For control mice, the respective paired AML/APL sample, which was used for co-culture, was thawed as described in the "Flow cytometry" section and depleted for $CD3^+$ cells. A total of 1×10^6 cells were transplanted via the retro-orbital sinus directly after thawing, and the rest of the cells were put in coculture with primary human MSCs for 48 hours. The same culture conditions were applied as for the macrophage co-culture. After 48 hours, cells were collected and counted to inject 200 to 350,000 primary blast cells via the retro-orbital sinus. Monitoring of leukemia engraftment and evaluation of AML/APL blast infiltration post-sacrifice was executed as described in the "In vivo intra-BM APL PDX model" section.

In vivo LT culture initiating cell assay

Engrafted primary APL blast cells, which were pre-cultured on M2d macrophages and induced fatal leukemia, were sorted post-sacrifice based on the human markers CD45, CD33, and CD117. Sorted APL blast cells from primary transplant were then transplanted via the retro-orbital sinus in secondary mice at different cell dosages: 1×10^3, 1×10^5, and 1.5×10^6. Control mice received different cell dosages as well: 5×10^5, 1×10^6, and 5×10^6 of APL samples at

diagnosis. The frequency of leukemic initiating stem cells was calculated with the ELDA software (*62*).

Murine in vivo preculture

Murine macrophages were generated and polarized in 20 × 100 petri dishes. Murine primary APL blasts were collected from hCG-PML-RARA mice (CD45.2$^+$ background), which developed APL. Once macrophages were polarized, the macrophages were washed and new RPMI supplemented with 10% FCS was added. Murine APL blast cells were then thawed, and 5 to 10 × 10^6 were put in co-culture for 48 hours. After 48 hours, suspension cells were collected and washed two times with PBS. Murine APL blast cells were counted, and 1 × 10^5 APL cells exposed to macrophages were set aside to evaluate the purity of these cells. Next, 1.5 × 10^5 murine APL cells were injected via retro-orbital sinus into sublethally irradiated (350 cGy) C57BL/6J.PepBoy recipients (CD45.1$^+$). For control mice, the respective paired murine APL sample, which was used for co-culture, was thawed, and a total of 1 × 10^6 cells were transplanted via the retro-orbital sinus directly after thawing. Chimerism levels were evaluated by measuring the CD45.2$^+$ marker by flow cytometry in blood obtained by submandibular bleeding. Mice were followed for OS analysis and euthanized when tumor reached ethical limits (>90% engraftment) or mice showed severe signs of illness. At the end of the experiment, animals were harvested and the BM was analyzed for the presence of early and late promyelocytes defined by CD34 and CD16/32 (CD34$^+$CD16/32$^+$, early pro/ CD34$^-$CD16/32$^+$, late pro) inside the population of lineage-negative cells (lineage markers defined by CD3e, CD19, B220, Ter119, NK1.1, CD4, and CD8) positive for CD117 and Gr1 intermediate (*63*, *64*).

OCR and ECAR measurements

OCR and ECAR were measured using a Seahorse XF96 analyzer (Seahorse Bioscience, Agilent, USA) at 37°C. For AML cell lines (CD45$^+$ cells) and sorted CD34$^+$ or CD117$^+$ from primary AML patients, 1 × 10^5 and 2 × 10^5 viable cells (DAPI$^-$) were seeded per well in poly--lysine (Sigma-Aldrich)–coated Seahorse XF96 plates in 180 μl of XF Assay Medium (modified DMEM, Seahorse Bioscience), respectively. For OCR measurements, XF Assay Medium was supplemented with 10 mM glucose, and 2.5 μM oligomycin A (port A), 2.5 μM FCCP [carbonyl cyanide-4-(trifluorometh oxy) phenylhydrazone)] (port B), and 2 μM antimycin A together with 2 μM rotenone (port C) were sequentially injected in 20-μl volume to measure basal and maximal OCR levels (all reagents from Sigma-Aldrich). For ECAR measurements, glucose-free XF Assay medium was added to the cells and 10 mM glucose (port A), 2.5 μM oligomycin A (port B), and 100 mM 2-deoxy--glucose (port C) (all reagents from Sigma-Aldrich). For measuring the metabolic activity after M2d or MS-5 coculture, we initially seeded 5 × 10^5 AML primary cells for 2 days and counted the remaining viable cells, loading equal amounts of cells. For Eto experiments, MS-5 and M2d macrophages were treated with Eto (50 μM) alone or in combination with VEN (250 nM) for 24 hours. After that, cells were washed twice with 1× PBS, primary AML blasts were added, and a co-culture for 24 hours was performed, to measure the OCR/ECAR in the AML cells. To exclude off-target effects from treated MS-5 or M2d macrophages on the exposed AML cells after coculture, AML cells were evaluated with the mitochondrial markers —MitoTracker Deep Red and tetramethylrhodamine, ethyl ester, perchlorate (Thermo Fisher Scientific) by FACS (LSRII). For measuring the metabolic consequences on M2d macrophages and AAMs upon Eto (50 μM), KPT-9274 (1.5 μM), and Daporinad (5 μM), cells were plated directly on seahorse plates (2 × 10^4 cells per well, in four technical replicates) and treated with the inhibitors for 48 hours prior the assay. All XF96 protocols consisted of four times mix (2 min) and measurement (2 min) cycles, allowing for determination of OCR at basal and also in between injections. Both basal and maximal OCR levels were calculated by assessing metabolic response of the cells in accordance with the manufacturer′s suggestions. The OCR measurements were normalized to the viable number of cells used for the assay.

Mitochondrial transfer assay

Mitochondrial transfer assays were performed as described by Moschoi *et al.* (*51*). Co-cultures of primary AML blasts with M2d macrophages and MS-5 confluent monolayer were performed in Gartners medium. Eto (50 μM; MedChemExpress, NL) treatment was performed in the MS5 and M2d macrophages 24 hours before the co-culture. Viability of the stromal cells was evaluated by DAPI staining. MS-5 and M2d macrophage MitoTracker loading was performed as follows: Confluent stromal cells were stained for 10 min with 2 μM MitoTracker Green FM and 1 μM MitoTracker Deep Red FM (Molecular Probes), washed twice, and left 72 hours to allow elimination of the unbound probe. Stromal cells were then washed twice again before initiating co-cultures with AML cells. As a quality control, conditioned medium of stained MS-5 and M2d macrophages 72 hours after staining was collected and used to stain AML cells, to evaluate the leakage of MitoTracker dyes.

In vivo homing assay

In total, 5 × 10^6 CD3$^+$ depleted APL cells were put in co-culture on M2d macrophages per well for 48 hours. After 48 hours, suspension APL cells were collected and counted. A total of 1 × 10^6 co-cultured APL blast cells were washed two times in serum-free medium at 450*g* for 5 min. APL cells were resuspended in 100 μl of serum-free medium and stained with 1 μl of Incucyte Cytolight Rapid Red Dye (0.33 μM) for 20 min at 37°C. Cells were then washed two times in medium with serum at 450*g* for 5 min. For the control group, cryopreserved MNC fractions of APL patient samples were thawed and depleted for CD3$^+$, and 1 × 10^6 cells were labeled with the Incucyte dye as described above. Labeled APL blast cells (after thawing and M2d cocultured) were transplanted via the retro-orbital sinus. In addition, 1 × 10^6 freshly thaw and co-cultured blast cells were set aside to stain for purity and measure the levels of CD49d, CD49e, and CD49f. All specimens were acquired by flow cytometry (FACS CantoII) and analyzed with the FlowJo software (Treestar Inc., USA). For each sample, a minimum of 20,000 events were acquired. Eighteen hours post-transplant, mice were euthanized, and legs were first flushed and then crushed to retrieve the maximum number of cells. BM cells were stained with DAPI and human CD45-APC, CD33-PE, and the Incucyte dye. A total of 5 × 10^6 DAPI-negative cells were acquired by flow cytometry (FACS CantoII) and analyzed with the FlowJo software (Treestar Inc., USA).

In vitro migration assay

Primary BM stromal cells (passage 3) were plated at a density of 1×10^5 per well in a transwell system in a six-well plate format. Migration assay was performed as previously described (*65*). Briefly, primary AML/APL blasts were co-cultured with M2d macrophages for 48 hours, and after the co-culture, diagnosis and co-cultured blasts were seeded (1×10^6 cells) in the upper chamber of the six-well plate and incubated at 37°C at 5% CO_2 for 18 hours to allow the migration upon the SDF-1 stimulus (produced by the MSCs in the lower chamber). After incubation, membranes were fixed with 99.9% methanol and stained with Violet Crystal. Colonies containing at least 50 cells were counted and considered as migrating cells. The values were then normalized to the diagnosis samples.

RNA-seq experiments and GO/GSEA analyses

RNA samples for sequencing were prepared for primary AML/APL blast cells at diagnosis and after 48 hours of coculture with MS-5 or M2d macrophages. Cells were collected after co-culture, and the human $CD34^+$ or $CD117^+$ (for *NPM1* mut AMLs and APL) was isolated for posterior RNA extraction. Total RNA was isolated using the RNeasy Micro Kit from Qiagen (Venlo, The Netherlands) according to the manufacturer′s recommendations. Initial quality check and RNA quantification of the samples were performed by automated gel electrophoresis on the 2200 TapeStation System (Agilent Technologies). Sequence libraries were generated using the KAPA RNA HyperPrep kit with riboErase (HMR) (Roche Sequencing and Life Sciences) according to the manufacturer′s protocol. The obtained cDNA fragment libraries were sequenced on an Illumina NextSeq500 using default parameters (25 M reads per sample). Sequencing reads were mapped to Hg38 with STAR version 2.7.3a (*66*) using the default parameters filtered for uniquely mapping reads with the following modifications: "--outFilterType BySJout --outFilterMultimapNmax 20 --outFilterMismatchNoverLmax 0.04 --outSAMtype BAM sorted --outSJfilterReads Unique --chimSegmentMin 20." While read counting per gene was calculated with STAR using the option: "--quantMode GeneCounts." Downstream analysis was performed in R version 4.0.5 (The CRAN project, www.r-project.org) using limma-voom (*67*) pipeline to generate the gene expression matrix. Briefly, our samples yielded libraries with a range from 10.8×10^6 to 4.22×10^7 (mean: 16.52×10^6 reads) uniquely mapped reads, and then we filtered out any samples whose library was ±2 SD from the mean to filter over-clustered samples. Read counts were normalized as counts per million (CPM) and $\log_2$ transformed ($\log_2$CPM). We used a filtering approach to eliminate non-expressed or marginally expressed genes from the 60,649 genes defined in ENSEMBL annotation. We retained genes that had a CPM > 8 in at least half of the samples of at least one of the experimental conditions considered. Thus, we retained 12,206 genes in our analysis.

We generated gene expression profiles by computing differentially expressed genes (DEGs). Our experimental design included comparisons of selected paired populations across two conditions (e.g., diagnosis × M2d samples using paired Wilcoxon rank sum analysis). We computed the $\log_2$ FCs, *P* values of differential expression (Wilcoxon), and the false discovery rate (FDR)–adjusted *P* values (Benjamini and Hochberg) of DEG in all the profiles. The statistical significance was set as FDR < 0.00001.

DEGs were clustered using unsupervised hierarchical clustering with Euclidean distances (complete) (stats package in R). Data are deposited at the GEO platform.

GSEA was performed using the Broad Institute software (http://software.broadinstitute.org/gsea/index.jsp). Gene ontology (GO) was evaluated using the gene ontology resource (http://geneontology.org/) and the BinGO plugin using the Cytoscape software v3.8.2 (NIGMS, USA). All genes from the RNA-seq of the different experimental group (diagnosis, MS-5 coculture and M2d coculture) cohort were pre-ranked according to their differential expression (FC). Enrichment scores were obtained with the Kolmogorov-Smirnov statistic, tested for significance using 1000 permutations, and normalized to consider the size of each gene set. As suggested by the GSEA, an FDR cutoff of 25% (FDR *q* value < 0.25) was used (*68*). Data visualization was performed with the ClustVis platform (*69*). RNA-sequencing data are available for download from the King′s Open Research Data System (KORDS) - DOI: 10.18742/22232140.

Lentiviral vectors and lentivirus production

Recombinant lentivirus encoding *FLT3*-ITD, *NPM1*cyt, and *BCR-ABL* fusion p210, overexpression of *MN1*, and the KD of *DNMT3A* (DNMT3A-KD) were generated using different lentiviral backbone plasmids as described in the resource table. Virus was produced in human embryonic kidney–293T cells according to the three-plasmid packaging procedure as described elsewhere (*70*). Lentiviral particles were concentrated using Amicon Ultra-15 centrifugal filter unit columns (Merck, CA, USA). Cells were sorted on the basis of their green fluorescent protein/mCherry protein expression, and sorted cells were used for in vitro assays. The efficiency of infection was further confirmed by gene expression quantification/detection of the mutant transcript. For the DNMT3A-KD experiments, a short hairpin RNA sequence that does not target human genes (referred to as scrambled) was used as a control.

Generation of lentiviral transduced CB macrophages

Peripheral blood mononuclear cells were isolated by a density gradient using Ficoll (Sigma-Aldrich) from CB. MNCs were washed once at 450*g* with PBS-EDTA (5 mM) and resuspended in 300 μl of PBS. Next, 100 μl of FcR blocking reagent and 100 μl of CD34 MicroBeads (Miltenyi Biotech) were added to the suspension and incubated for 30 min at 4°C. After incubation, cells were washed for 10 min at 450*g* and resuspended in 2 ml of PBS-EDTA (5 mM). Cells were passed through a cell strainer (70 μm) and isolated by magnetic separation on the autoMACS (Program: Possedels, Miltenyi Biotech). The purity of the isolated cells was routinely evaluated by FACS and in the range of 85 to 95%.

CB-isolated $CD34^+$ were next expanded in Stem Cell II medium supplemented with stem cell factor (100 ng/ml), FLT3 ligand (50 ng/ml), GM-CSF (30 ng/ml), and IL-6 (10 ng/ml). Five days later, cells were collected and transduced with concentrated virus containing the empty vector construct or different oncogenic lentivectors as described above. After transduction, the cells were cultured in Iscove′s modified Dulbecco′s medium (IMDM) supplemented with 20% FCS and M-CSF (50 ng/ml) to induce macrophage differentiation for 21 days.

Phagocytosis assay by microscopy

Macrophages, which were generated in a six-well plate, were detached with TrypLE, and 1×10^4 macrophages were seeded in a flat-bottom 96-well plate to reach a confluence of approximately 80%. Macrophages were then incubated overnight to allow adherence. Cryopreserved MNC fractions of AML cells were thaw and $CD3^+$ depleted. For the phagocytosis at day 0, a total of 1×10^5 AML cells were washed two times in serum-free medium at 450*g* for 5 min, resuspended in 100 μl, and stained with 1 μl of Incucyte Cytolight Rapid Red Dye (0.33 μM) or CSFE AF488 (concentration, Thermo Fisher Scientific). Cells were incubated for 20 min at 37°C and washed two times with medium supplemented with serum. A total of 3×10^4 were cocultured with macrophages in a 96-well plate and incubated for 3 hours at 37°C and 5% CO_2. After 3 hours of incubation, AML cells were gently removed by washing with PBS three times. To visualize macrophages, residual cells were stained with CD11b-FITC (1 μg/ml) (when AML cells were labeled with Incucyte Red Dye) or CD11b-AF594 (1 μg/ml) (when AML cells labeled with CSFE AF488) 30 min at room temperature in the dark. After 30 min, macrophages were fixed with 2% paraformaldehyde, and three pictures of randomly chosen fields of view were taken by the EVOS Cell Imaging System (Thermo Fisher Scientific). The percentage of phagocytosis was equal to the number of macrophages containing labeled AML cells per 100 macrophages. For phagocytosis at day 2, a total of 5×10^5 to 1×10^6 AML cells were put in co-culture with either M2d macrophages or MS-5 cells seeded in a 12-well plate for 48 hours. The co-cultures were performed in Gartner′s medium. After 48 hours of coculture, AML cells were collected, and a phagocytosis assay was performed as described above.

Phagocytosis assay by flow cytometry

Macrophages were detached, and target cells (MV4-11 cells for the AAM phagocytosis) were stained with CSFE as described in the "Phagocytosis assay by microscopy" section. A total of 3×10^4 macrophages and 9×10^4 target cells (ratio 1:3, macrophage:target cell) were mixed together in a FACS tube and incubated for 3 hours at 37°C and 5% CO_2. After 3 hours of incubation, cells were directly stained with CD11b-APC and incubated for another 20 min at 37°C and 5% CO_2. Cells were then washed and resuspended in PBS. All specimens were acquired by flow cytometry (BD LSR II) and analyzed with the FlowJo software (Treestar Inc., USA). For each sample, a minimum of 10,000 events inside the $CD11b^+$ population were acquired.

AAM isolation and culture

Primary AML samples were thawed as described in the "Flow cytometry" section. After thawing, 1.5 million cells/ml were plated in liquid culture in a six-well dish in Gartner′s medium supplemented with G-SCF, TPO, and IL-3 at a concentration of 20 ng/ml. Two days after liquid culture, the adhered plastic AML macrophage fraction was isolated by removal of the supernatant comprehending AML blast cells and lymphocytes. Macrophages were cultured 2 to 3days longer in Gartner′s medium supplemented with G-CSF, TPO, and IL-3 at a concentration of 20 ng/ml before being used for experiments.

CALR differential gene/protein expression analysis and GSEA

The TCGA transcriptome dataset for patients with AML was retrieved from the Firebrowse data portal (www.firebrowse.org). For the purpose of the analysis, patients with APL were excluded (since they represent the group with the highest *CALR* expression). To evaluate the profile of CALR high and low AML samples in HSPC populations, we used our GSE30029 cohort (*25*), which performed transcriptome analysis of sorted $CD34^+$ cells to exclude the contributions from the nonleukemic blasts. Next, all patients with AML were ranked from highest to lowest *CALR* expression. The DEG analysis was performed on the 10 patients with the highest and lowest expression of *CALR* using the "DESeq" package (*71*) in the R v4.1.3 software screen. The mRNA with $\log_2FC > 1.5$ and *P* adjusted value < 0.05 were considered as differentially expressed mRNA between $CALR^{high}$ and $CALR^{low}$ patients. Principal components analysis plot and heatmap were generated using the ggplot2 packages in the R platform for the obtained differentially expressed RNAs. The GSEA was performed as described in the "RNA-seq experiments and GO/GSEA analyses" section.

Proteome of AML blasts and correlation analysis with the macrophage landscape

Proteomic analysis was performed as previously described (available at PRIDE under PXD030463) (*2*). Proteomic landscape of the sorted AML blasts ($CD34^+$ or $CD117^+$ in case of *NPM1* mutant or $CD34^-$ AML blasts) was correlated with the macrophage landscape of the same patient sample, determined as described in the "Flow cytometry" section.

Enzymatic activity assays

Both extracellular lactate and glucose concentrations were determined from the cell culture medium by monitoring NAD(P)H increase occurring during specific enzymatic reactions for each metabolite at 340-nm wavelength, as described elsewhere (*72*, *73*). Briefly, extracellular lactate concentrations were determined by the lactate dehydrogenase (LDH) enzymatic reaction in the cell culture medium taken at 0 hours and after co-culture of tumor cells with MS-5 or M2d macrophages, for 48 hours of incubation. Cells were seeded in liquid culture after cocultures, and culture medium was taken after 24 hours. Extracellular lactate was converted LDH (Sigma-Aldrich) reaction in freshly prepared 25 mM NAD^+ and LDH (87.7 U/ml) in 0.4 M hydrazine (Sigma-Aldrich)/0.5 M glycine assay buffer (pH 9). Twenty microliters of samples (diluted according to the standard curve) and sodium-lactate (Sigma-Aldrich) standards were pipetted into 130 μl of reagent mix in a 96-well plate format, and the reaction was carried out for 30 min at 37°C. Glucose consumption was detected using an enzymatic reagent mix consisting of 75 μl of 100 mM Piper buffer, 2.5 μl of 40 mM nicotinamide adenine dinucleotide phosphate (NADP), 2 μl of 10 mM ATP, 1 μl of 500 mM $MgSO_4$, 0.15 μl of hexokinase, 0.15 μl of glucose-6-phosphate-dehyrogenase, and 44.3 μl of H_20 per well and was prepared, and 125 μl was added to both medium and glucose standard wells. The plate was incubated for 30 min at 37°C. Values of consumption and release of extracellular metabolites for each sample were normalized by cell number and incubation time considering the exponential growth curve. The NAD/NADH quantification colorimetric kit (Abcam, CB, UK) was used to quantify total NAD levels in M1- and M2d-polarized

macrophages, isolated from PB samples, treated with KPT-9274 (1.5 μM) and Daporinad (5 μM) for 48 hours before the measurements. Assay was performed as previously described (*33*). Briefly, macrophages were detached using TrypLE solution and washed twice in IMDM + 20% FCS to remove any residual TrypLE reagent. After that, cells were washed twice in PBS, counted, and pelleted by centrifugation. Cell pellets were immediately used for analysis, following the manufacturer's instructions. The total NAD level in each sample was measured and normalized on the basis of the input cell number.

Ex vivo drug screening in primary AML samples

Cryopreserved mononuclear cell fractions of patients with AML were thawed and prepared, as previously described in the "Flow cytometry" section, and resuspended in IMDM + 20% FCS, +G-CSF (20 ng/ml), IL-3, and N-plate. Cells were plated at a cellular density of 1.5 million cells/ml for 48 hours, to remove cellular debris that remained after the thawing procedure. For the ex vivo drug screening, cells were washed once in IMDM + 20% FCS and plated at 1.5×10^5 cells/ml in 48-well plates and treated with a dose range of the different compounds used to evaluate the cytotoxic effects on leukemic blasts, as well as on the tumor-supportive microenvironment. To analyze the myeloid fraction of the AML/APL bulk treated cells, treated mononuclear cells were blocked with human FcR blocking reagent (Miltenyi Biotec) for 5 min and stained with the following antibodies: CD45-APCCy7, CD34-PE (or CD117-PE for CD34- samples), CD14-PerCP, CD163-Pe-Cy7, CD206-BV421, and CD80-APC for 20 min at 4°C. After incubation, cells were washed once in PBS and, in the end, resuspended in IMDM + 20% FCS supplemented with 10% of $Ca2^+$ buffer (10×, BD Biosciences, CA, USA) plus annexin V FITC (BioLegend, CA, USA). Fluorescence was measured on the BD LSRII and analyzed using FlowJo (Tree Star Inc.). The apoptosis induction was evaluated in the leukemic blast population ($CD34^+$ or $CD117^+$), as well as in the more mature myeloid population (AAMs). A more mature myeloid population was detected on the basis of the CD45 staining positive for CD14 and negative for CD34/CD117. The different macrophage populations were then analyzed for their expression of the M1 marker CD80 and the M2 markers CD163 and CD206. To identify possible confounders to the association between drug sensitivity and the levels of AAMs detected at diagnosis, we performed multivariate logistic regression analysis comparing all the drugs included in the screening and the main genetic mutations observed in the patients (*FLT3*-ITD, *NPM1*, *CEBPA*, *IDH1*/2, *SRSF2*, *SF3B1*, *U2AF1*, *RAS* mutations, *RUNX1*, *TP53*, and *DNMT3A*), age, and sex, as confounders.

Supplementary Materials

This PDF file includes:
Figs. S1 to S6
Resources Table
Legend for data S1

Other Supplementary Material for this manuscript includes the following:
Data S1

View/request a protocol for this paper from *Bio-protocol*.

REFERENCES AND NOTES

1. H. Döhner, E. Estey, D. Grimwade, S. Amadori, F. R. Appelbaum, T. Büchner, H. Dombret, B. L. Ebert, P. Fenaux, R. A. Larson, R. L. Levine, F. Lo-Coco, T. Naoe, D. Niederwieser, G. J. Ossenkoppele, M. Sanz, J. Sierra, M. S. Tallman, H.-F. Tien, A. H. Wei, B. Löwenberg, C. D. Bloomfield, Diagnosis and management of AML in adults: 2017 ELN recommendations from an international expert panel. *Blood* **129**, 424–447 (2017).
2. B. de Boer, J. Prick, M. G. Pruis, P. Keane, M. R. Imperato, J. Jaques, A. Z. Brouwers-Vos, S. M. Hogeling, C. M. Woolthuis, M. T. Nijk, A. Diepstra, S. Wandinger, M. Versele, R. M. Attar, P. N. Cockerill, G. Huls, E. Vellenga, A. B. Mulder, C. Bonifer, J. J. Schuringa, Prospective isolation and characterization of genetically and functionally distinct AML subclones. *Cancer Cell* **34**, 674–689.e8 (2018).
3. L. A. Miles, R. L. Bowman, T. R. Merlinsky, I. S. Csete, A. T. Ooi, R. Durruthy-Durruthy, M. Bowman, C. Famulare, M. A. Patel, P. Mendez, C. Ainali, B. Demaree, C. L. Delley, A. R. Abate, M. Manivannan, S. Sahu, A. D. Goldberg, K. L. Bolton, A. Zehir, R. Rampal, M. P. Carroll, S. E. Meyer, A. D. Viny, R. L. Levine, Single-cell mutation analysis of clonal evolution in myeloid malignancies. *Nature* **587**, 477–482 (2020).
4. K. Morita, F. Wang, K. Jahn, T. Hu, T. Tanaka, Y. Sasaki, J. Kuipers, S. Loghavi, S. A. Wang, Y. Yan, K. Furudate, J. Matthews, L. Little, C. Gumbs, J. Zhang, X. Song, E. Thompson, K. P. Patel, C. E. Bueso-Ramos, C. D. DiNardo, F. Ravandi, E. Jabbour, M. Andreeff, J. Cortes, K. Bhalla, G. Garcia-Manero, H. Kantarjian, M. Konopleva, D. Nakada, N. Navin, N. Beerenwinkel, P. A. Futreal, K. Takahashi, Clonal evolution of acute myeloid leukemia revealed by high-throughput single-cell genomics. *Nat. Commun.* **11**, 5327 (2020).
5. M. H. G. P. Raaijmakers, S. Mukherjee, S. Guo, S. Zhang, T. Kobayashi, J. A. Schoonmaker, B. L. Ebert, F. Al-Shahrour, R. P. Hasserjian, E. O. Scadden, Z. Aung, M. Matza, M. Merkenschlager, C. Lin, J. M. Rommens, D. T. Scadden, Bone progenitor dysfunction induces myelodysplasia and secondary leukaemia. *Nature* **464**, 852–857 (2010).
6. A. Colmone, M. Amorim, A. L. Pontier, S. Wang, E. Jablonski, D. A. Sipkins, Leukemic cells create bone marrow niches that disrupt the behavior of normal hematopoietic progenitor cells. *Science* **322**, 1861–1865 (2008).
7. S. J. Turley, V. Cremasco, J. L. Astarita, Immunological hallmarks of stromal cells in the tumour microenvironment. *Nat. Rev. Immunol.* **15**, 669–682 (2015).
8. S. J. Morrison, D. T. Scadden, The bone marrow niche for haematopoietic stem cells. *Nature* **505**, 327–334 (2014).
9. S. W. Lane, D. T. Scadden, D. G. Gilliland, The leukemic stem cell niche: Current concepts and therapeutic opportunities. *Blood* **114**, 1150–1157 (2009).
10. A. Rizo, E. Vellenga, G. de Haan, J. J. Schuringa, Signaling pathways in self-renewing hematopoietic and leukemic stem cells: Do all stem cells need a niche? *Hum. Mol. Genet.* **15**suppl_2, R210–R219 (2006).
11. A. Chow, D. Lucas, A. Hidalgo, S. Méndez-Ferrer, D. Hashimoto, C. Scheiermann, M. Battista, M. Leboeuf, C. Prophete, N. van Rooijen, M. Tanaka, M. Merad, P. S. Frenette, Bone marrow $CD169^+$ macrophages promote the retention of hematopoietic stem and progenitor cells in the mesenchymal stem cell niche. *J. Exp. Med.* **208**, 261–271 (2011).
12. J. Hur, J.-I. Choi, H. Lee, P. Nham, T.-W. Kim, C.-W. Chae, J.-Y. Yun, J.-A. Kang, J. Kang, S. E. Lee, C.-H. Yoon, K. Boo, S. Ham, T.-Y. Roh, J. K. Jun, H. Lee, S. H. Baek, H.-S. Kim, CD82/KAI1 maintains the dormancy of long-term hematopoietic stem cells through interaction with DARC-expressing macrophages. *Cell Stem Cell* **18**, 508–521 (2016).
13. R. N. Jacobsen, C. E. Forristal, L. J. Raggatt, B. Nowlan, V. Barbier, S. Kaur, N. van Rooijen, I. G. Winkler, A. R. Pettit, J.-P. Levesque, Mobilization with granulocyte colony-stimulating factor blocks medullar erythropoiesis by depleting $F4/80^+VCAM1^+CD169^+ER\text{-}HR3^+Ly6G^+$ erythroid island macrophages in the mouse. *Exp. Hematol.* **42**, 547–561.e4 (2014).
14. A. Chow, M. Huggins, J. Ahmed, D. Hashimoto, D. Lucas, Y. Kunisaki, S. Pinho, M. Leboeuf, C. Noizat, N. van Rooijen, M. Tanaka, Z. J. Zhao, A. Bergman, M. Merad, P. S. Frenette, $CD169^+$ macrophages provide a niche promoting erythropoiesis under homeostasis and stress. *Nat. Med.* **19**, 429–436 (2013).
15. F. Mussai, C. de Santo, I. Abu-Dayyeh, S. Booth, L. Quek, R. M. McEwen-Smith, A. Qureshi, F. Dazzi, P. Vyas, V. Cerundolo, Acute myeloid leukemia creates an arginase-dependent immunosuppressive microenvironment. *Blood* **122**, 749–758 (2013).
16. Y. S. Al-Matary, L. Botezatu, B. Opalka, J. M. Hönes, R. F. Lams, A. Thivakaran, J. Schütte, R. Köster, K. Lennartz, T. Schroeder, R. Haas, U. Dührsen, C. Khandanpour, Acute myeloid leukemia cells polarize macrophages towards a leukemia supporting state in a Growth factor independence 1 dependent manner. *Haematologica* **101**, 1216–1227 (2016).
17. R. Guo, M. Lü, F. Cao, G. Wu, F. Gao, H. Pang, Y. Li, Y. Zhang, H. Xing, C. Liang, T. Lyu, C. du, Y. Li, R. Guo, X. Xie, W. Li, D. Liu, Y. Song, Z. Jiang, Single-cell map of diverse immune phenotypes in the acute myeloid leukemia microenvironment. *Biomark. Res.* **9**, 15 (2021).
18. P. van Galen, V. Hovestadt, M. H. Wadsworth II, T. K. Hughes, G. K. Griffin, S. Battaglia, J. A. Verga, J. Stephansky, T. J. Pastika, J. Lombardi Story, G. S. Pinkus, O. Pozdnyakova, I. Galinsky, R. M. Stone, T. A. Graubert, A. K. Shalek, J. C. Aster, A. A. Lane, B. E. Bernstein, Single-cell RNA-seq reveals AML hierarchies relevant to disease progression and immunity. *Cell* **176**, 1265–1281.e24 (2019).

19. Z.-J. Xu, Y. Gu, C.-Z. Wang, Y. Jin, X.-M. Wen, J.-C. Ma, L.-J. Tang, Z.-W. Mao, J. Qian, J. Lin, The M2 macrophage marker *CD206*: A novel prognostic indicator for acute myeloid leukemia. *Onco. Targets. Ther.* **9**, 1683347 (2020).
20. M. H. Kramer, Q. Zhang, R. Sprung, R. B. Day, P. Erdmann-Gilmore, Y. Li, Z. Xu, N. M. Helton, D. R. George, Y. Mi, P. Westervelt, J. E. Payton, S. M. Ramakrishnan, C. A. Miller, D. C. Link, J. F. DiPersio, M. J. Walter, R. R. Townsend, T. J. Ley, Proteomic and phosphoproteomic landscapes of acute myeloid leukemia. *Blood* **140**, 1533–1548 (2022).
21. The Cancer Genome Atlas Research Network, Genomic and epigenomic landscapes of adult de novo acute myeloid leukemia. *N. Engl. J. Med.* **368**, 2059–2074 (2013).
22. A. Reinisch, D. Thomas, M. R. Corces, X. Zhang, D. Gratzinger, W.-J. Hong, K. Schallmoser, D. Strunk, R. Majeti, A humanized bone marrow ossicle xenotransplantation model enables improved engraftment of healthy and leukemic human hematopoietic cells. *Nat. Med.* **22**, 812–821 (2016).
23. S. Jaiswal, C. H. M. Jamieson, W. W. Pang, C. Y. Park, M. P. Chao, R. Majeti, D. Traver, N. van Rooijen, I. L. Weissman, CD47 is upregulated on circulating hematopoietic stem cells and leukemia cells to avoid phagocytosis. *Cell* **138**, 271–285 (2009).
24. A. A. Barkal, R. E. Brewer, M. Markovic, M. Kowarsky, S. A. Barkal, B. W. Zaro, V. Krishnan, J. Hatakeyama, O. Dorigo, L. J. Barkal, I. L. Weissman, CD24 signalling through macrophage Siglec-10 is a target for cancer immunotherapy. *Nature* **572**, 392–396 (2019).
25. H. J. M. de Jonge, C. M. Woolthuis, A. Z. Vos, A. Mulder, E. van den Berg, P. M. Kluin, K. van der Weide, E. S. J. M. de Bont, G. Huls, E. Vellenga, J. J. Schuringa, Gene expression profiling in the leukemic stem cell-enriched $CD34^+$ fraction identifies target genes that predict prognosis in normal karyotype AML. *Leukemia* **25**, 1825–1833 (2011).
26. C. Pabst, A. Bergeron, V.-P. Lavallée, J. Yeh, P. Gendron, G. L. Norddahl, J. Krosl, I. Boivin, E. Deneault, J. Simard, S. Imren, G. Boucher, K. Eppert, T. Herold, S. K. Bohlander, K. Humphries, S. Lemieux, J. Hébert, G. Sauvageau, F. Barabé, GPR56 identifies primary human acute myeloid leukemia cells with high repopulating potential in vivo. *Blood* **127**, 2018–2027 (2016).
27. E. Coustan-Smith, G. Song, S. Shurtleff, A. E.-J. Yeoh, W. J. Chng, S. P. Chen, J. E. Rubnitz, C.-H. Pui, J. R. Downing, D. Campana, Universal monitoring of minimal residual disease in acute myeloid leukemia. *JCI Insight* **3**, e98561 (2018).
28. E. Kroon, J. Krosl, U. Thorsteinsdottir, S. Baban, A. M. Buchberg, G. Sauvageau, Hoxa9 transforms primary bone marrow cells through specific collaboration with Meis1a but not Pbx1b. *EMBO J.* **17**, 3714–3725 (1998).
29. C. Larrue, N. Guiraud, P.-L. Mouchel, M. Dubois, T. Farge, M. Gotanègre, C. Bosc, E. Saland, M.-L. Nicolau-Travers, M. Sabatier, N. Serhan, A. Sahal, E. Boet, S. Mouche, Q. Heydt, N. Aroua, L. Stuani, T. Kaoma, L. Angenendt, J.-H. Mikesch, C. Schliemann, F. Vergez, J. Tamburini, C. Récher, J.-E. Sarry, Adrenomedullin-CALCRL axis controls relapse-initiating drug tolerant acute myeloid leukemia cells. *Nat. Commun.* **12**, 422 (2021).
30. F. Kocabas, J. Zheng, S. Thet, N. G. Copeland, N. A. Jenkins, R. J. DeBerardinis, C. Zhang, H. A. Sadek, Meis1 regulates the metabolic phenotype and oxidant defense of hematopoietic stem cells. *Blood* **120**, 4963–4972 (2012).
31. M. Nomura, J. Liu, I. I. Rovira, E. Gonzalez-Hurtado, J. Lee, M. J. Wolfgang, T. Finkel, Fatty acid oxidation in macrophage polarization. *Nat. Immunol.* **17**, 216–217 (2016).
32. G. Hu, Y. Su, B. H. Kang, Z. Fan, T. Dong, D. R. Brown, J. Cheah, K. D. Wittrup, J. Chen, High-throughput phenotypic screen and transcriptional analysis identify new compounds and targets for macrophage reprogramming. *Nat. Commun.* **12**, 773 (2021).
33. A. Subedi, Q. Liu, D. M. Ayyathan, D. Sharon, S. Cathelin, M. Hosseini, C. Xu, V. Voisin, G. D. Bader, A. D'Alessandro, E. R. Lechman, J. E. Dick, M. D. Minden, J. C. Y. Wang, S. M. Chan, Nicotinamide phosphoribosyltransferase inhibitors selectively induce apoptosis of AML stem cells by disrupting lipid homeostasis. *Cell Stem Cell* **28**, 1851–1867.e8 (2021).
34. A. Mantovani, F. Marchesi, A. Malesci, L. Laghi, P. Allavena, Tumour-associated macrophages as treatment targets in oncology. *Nat. Rev. Clin. Oncol.* **14**, 399–416 (2017).
35. J. M. Klco, D. H. Spencer, C. A. Miller, M. Griffith, T. L. Lamprecht, M. O'Laughlin, C. Fronick, V. Magrini, R. T. Demeter, R. S. Fulton, W. C. Eades, D. C. Link, T. A. Graubert, M. J. Walter, E. R. Mardis, J. F. Dipersio, R. K. Wilson, T. J. Ley, Functional heterogeneity of genetically defined subclones in acute myeloid leukemia. *Cancer Cell* **25**, 379–392 (2014).
36. S. Avagyan, J. E. Henninger, W. P. Mannherz, M. Mistry, J. Yoon, S. Yang, M. C. Weber, J. L. Moore, L. I. Zon, Resistance to inflammation underlies enhanced fitness in clonal hematopoiesis. *Science* **374**, 768–772 (2021).
37. P. G. Kim, A. Niroula, V. Shkolnik, M. McConkey, A. E. Lin, M. Słabicki, J. P. Kemp, A. Bick, C. J. Gibson, G. Griffin, A. Sekar, D. J. Brooks, W. J. Wong, D. N. Cohen, M. M. Uddin, W. J. Shin, J. Pirruccello, J. M. Tsai, M. Agrawal, D. P. Kiel, M. L. Bouxsein, J. B. Richards, D. M. Evans, M. N. Wein, J. F. Charles, S. Jaiswal, P. Natarajan, B. L. Ebert, Dnmt3a-mutated clonal hematopoiesis promotes osteoporosis. *J. Exp. Med.* **218**, e20211872 (2021).
38. A. Yeaton, G. Cayanan, S. Loghavi, I. Dolgalev, E. M. Leddin, C. E. Loo, H. Torabifard, D. Nicolet, J. Wang, K. Corrigan, V. Paraskevopoulou, D. T. Starczynowski, E. Wang, O. Abdel-Wahab, A. D. Viny, R. M. Stone, J. C. Byrd, O. A. Guryanova, R. M. Kohli, G. A. Cisneros, A. Tsirigos, A. K. Eisfeld, I. Aifantis, M. Guillamot, The impact of inflammation-induced tumor plasticity during myeloid transformation. *Cancer Discov.* **12**, 2392–2413 (2022).
39. X.-Y. He, C. Xiang, C.-X. Zhang, Y.-Y. Xie, L. Chen, G.-X. Zhang, Y. Lu, G. Liu, p53 in the myeloid lineage modulates an inflammatory microenvironment limiting initiation and invasion of intestinal tumors. *Cell Rep.* **13**, 888–897 (2015).
40. T. Cooks, I. S. Pateras, L. M. Jenkins, K. M. Patel, A. I. Robles, J. Morris, T. Forshew, E. Appella, V. G. Gorgoulis, C. C. Harris, Mutant p53 cancers reprogram macrophages to tumor supporting macrophages via exosomal miR-1246. *Nat. Commun.* **9**, 771 (2018).
41. T. Grob, A. S. A. al Hinai, M. A. Sanders, F. G. Kavelaars, M. Rijken, P. L. Gradowska, B. J. Biemond, D. A. Breems, J. Maertens, M. van Marwijk Kooy, T. Pabst, O. de Weerdt, G. J. Ossenkoppele, A. A. van de Loosdrecht, G. A. Huls, J. J. Cornelissen, H. B. Beverloo, B. Löwenberg, M. Jongen-Lavrencic, P. J. M. Valk, Molecular characterization of mutant TP53 acute myeloid leukemia and high-risk myelodysplastic syndrome. *Blood* **139**, 2347–2354 (2022).
42. H. L. Thompson, N. van Rooijen, B. T. McLelland, J. O. Manilay, $F4/80^+$ host macrophages are a barrier to murine embryonic stem cell-derived hematopoietic progenitor engraftment in vivo. *J. Immunol. Res.* **2016**, 2414906 (2016).
43. J. A. Moore, J. J. Mistry, C. Hellmich, R. H. Horton, E. E. Wojtowicz, A. Jibril, M. Jefferson, T. Wileman, N. Beraza, K. M. Bowles, S. A. Rushworth, LC3-associated phagocytosis in bone marrow macrophages suppresses acute myeloid leukemia progression through STING activation. *J. Clin. Invest.* **132**, e153157 (2022).
44. F. Mussai, S. Egan, J. Higginbotham-Jones, T. Perry, A. Beggs, E. Odintsova, J. Loke, G. Pratt, K. P. U, A. Lo, M. Ng, P. Kearns, P. Cheng, C. de Santo, Arginine dependence of acute myeloid leukemia blast proliferation: A novel therapeutic target. *Blood* **125**, 2386–2396 (2015).
45. M. P. Chao, S. Jaiswal, R. Weissman-Tsukamoto, A. A. Alizadeh, A. J. Gentles, J. Volkmer, K. Weiskopf, S. B. Willingham, T. Raveh, C. Y. Park, R. Majeti, I. L. Weissman, Calreticulin is the dominant pro-phagocytic signal on multiple human cancers and is counterbalanced by CD47. *Sci. Transl. Med.* **2**, 63ra94 (2010).
46. M. Michalak, J. Groenendyk, E. Szabo, L. I. Gold, M. Opas, Calreticulin, a multi-process calcium-buffering chaperone of the endoplasmic reticulum. *Biochem. J.* **417**, 651–666 (2009).
47. A. Han, C. Li, T. Zahed, M. Wong, I. Smith, K. Hoedel, D. Green, A. D. Boiko, Calreticulin is a critical cell survival factor in malignant neoplasms. *PLoS Biol.* **17**, e3000402 (2019).
48. L. M. Scott, G. V. Priestley, T. Papayannopoulou, Deletion of alpha4 integrins from adult hematopoietic cells reveals roles in homeostasis, regeneration, and homing. *Mol. Cell. Biol.* **23**, 9349–9360 (2003).
49. T. Yahata, K. Ando, T. Sato, H. Miyatake, Y. Nakamura, Y. Muguruma, S. Kato, T. Hotta, A highly sensitive strategy for SCID-repopulating cell assay by direct injection of primitive human hematopoietic cells into NOD/SCID mice bone marrow. *Blood* **101**, 2905–2913 (2003).
50. S. J. Wattrus, M. L. Smith, C. P. Rodrigues, E. J. Hagedorn, J. W. Kim, B. Budnik, L. I. Zon, Quality assurance of hematopoietic stem cells by macrophages determines stem cell clonality. *Science* **377**, 1413–1419 (2022).
51. R. Moschoi, V. Imbert, M. Nebout, J. Chiche, D. Mary, T. Prebet, E. Saland, R. Castellano, L. Pouyet, Y. Collette, N. Vey, C. Chabannon, C. Recher, J.-E. Sarry, D. Alcor, J.-F. Peyron, E. Griessinger, Protective mitochondrial transfer from bone marrow stromal cells to acute myeloid leukemic cells during chemotherapy. *Blood* **128**, 253–264 (2016).
52. Y. Luo, L. Shao, J. Chang, W. Feng, Y. L. Liu, M. H. Cottler-Fox, P. D. Emanuel, M. Hauer-Jensen, I. D. Bernstein, L. Liu, X. Chen, J. Zhou, P. J. Murray, D. Zhou, M1 and M2 macrophages differentially regulate hematopoietic stem cell self-renewal and ex vivo expansion. *Blood Adv.* **2**, 859–870 (2018).
53. T. Saha, C. Dash, R. Jayabalan, S. Khiste, A. Kulkarni, K. Kurmi, J. Mondal, P. K. Majumder, A. Bardia, H. L. Jang, S. Sengupta, Intercellular nanotubes mediate mitochondrial trafficking between cancer and immune cells. *Nat. Nanotechnol.* **17**, 98–106 (2022).
54. Y. Hao, S. Hao, E. Andersen-Nissen, W. M. Mauck III, S. Zheng, A. Butler, M. J. Lee, A. J. Wilk, C. Darby, M. Zager, P. Hoffman, M. Stoeckius, E. Papalexi, E. P. Mimitou, J. Jain, A. Srivastava, T. Stuart, L. M. Fleming, B. Yeung, A. J. Rogers, J. M. McElrath, C. A. Blish, R. Gottardo, P. Smibert, R. Satija, Integrated analysis of multimodal single-cell data. *Cell* **184**, 3573–3587.e29 (2021).
55. S. Triana, D. Vonficht, L. Jopp-Saile, S. Raffel, R. Lutz, D. Leonce, M. Antes, P. Hernández-Malmierca, D. Ordoñez-Rueda, B. Ramasz, T. Boch, J.-C. Jann, D. Nowak, W.-K. Hofmann, C. Müller-Tidow, D. Hübschmann, T. Alexandrov, V. Benes, A. Trumpp, M. Paulsen, L. Velten, S. Haas, Single-cell proteo-genomic reference maps of the hematopoietic system enable the purification and massive profiling of precisely defined cell states. *Nat. Immunol.* **22**, 1577–1589 (2021).
56. S. Aibar, C. B. González-Blas, T. Moerman, V. A. Huynh-Thu, H. Imrichova, G. Hulselmans, F. Rambow, J.-C. Marine, P. Geurts, J. Aerts, J. van den Oord, Z. K. Atak, J. Wouters, S. Aerts, SCENIC: Single-cell regulatory network inference and clustering. *Nat. Methods* **14**, 1083–1086 (2017).